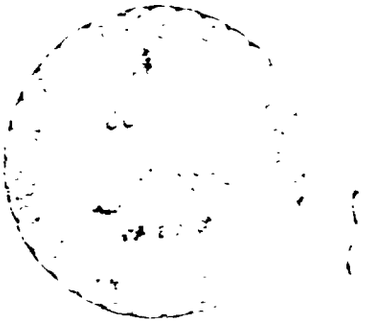

THE UNIVERSITY OF KANSAS CENTER FOR RESEARCH, INC.
2291 Irving Hill Drive—Campus West
Lawrence, Kansas 66045

Final Report
on

PIONEER VENUS PROBE MODELS

INSTRUMENTED DROP TESTS

August 1978

KU-FRL 333-1

NASA Ames Research Center

Contract NAS2-9414

Mr. Alvin Seiff, Technical Officer

by

Vincent U. Muirhead
Principal Investigator
The University of Kansas

TABLE OF CONTENTS

LIST OF SYMBOLS

M	Mach Number
R_N	Reynolds number (based on separation ring diameter)
a	Acceleration
x	Axis of sideslip (body axis)
y	Axis of pitch (body axis)
z	Axis of spin (body axis) or flight path (wind axis)
α	Angle of attack about the y axis (angle between the z body axis and the relative wind in the x, z plane)
β	Angle of sideslip about the x axis (angle between the z body axis and the relative wind in the y, z plane)
C_L	Coefficient of lift (wind axis)
C_D	Coefficient of drag (wind axis)
C_{SF}	Coefficient of side force

Subscripts

x,y	x and y body axes
w	wind axes

LIST OF FIGURES

LIST OF TABLES

ACKNOWLEDGEMENTS

The advice and comments of Mr. Alvin Seiff, NASA Ames Research Center, are gratefully acknowledged. The following staff and students participated in various phases of the model build-up, tests and data reduction:

David Nelson

Howard Henry

Douglas Carlson

Charles Hughes

Steven Erickson

Keith Braman

Robert Rodgers

Mike Griswold

SUMMARY

Models of both the small and large Pioneer Venus probes which are scheduled to be launched during 7-27 August, 1978, were dropped from a helicopter to simulate the conditions of Mach and Reynolds numbers to be encountered by the Pioneer Venus probes upon entry into the Venus atmosphere.

The models were dropped at an average Mach number of .10 and at an average Reynolds number of 2.84×10^6 for the small probe and 2.90×10^6 for the large probe. After the large amplitude launching oscillations had been damped, the small probe oscillations in angle of attack and in sideslip were generally less than 2 degrees. The large probe oscillations were generally less than 10 degrees. Both exhibited distinct frequencies. The motion of the small probe in a place perpendicular to the z axis was random while the large probe rotated (corkscrewed) at 1.1 cycles per second about the z axis.

The average drag coefficients of the probe models were .714 for the small probe and .663 for the large probe.

1. INTRODUCTION

During 7-24 August, 1978, a multiprobe spacecraft is scheduled to be launched on a trajectory from Earth to Venus. The probe bus will launch one large probe and three small probes prior to making upper atmosphere measurements and burning up. The large probe will make detailed measurements of the lower atmosphere. The small probes will provide additional data for the general atmospheric circulation.

In order to obtain accurate results the aerodynamic characteristics of the probes must be known. Although wind tunnel tests have been conducted to determine the drag and lift coefficients and the buffeting characteristics,[1,2] these data do not reflect the effects of the buffeting which occurs in a free flight fall. The very nature of the wind tunnel mounting system is such that the natural vibrations of the mounting system overpower and mask the aerodynamic buffeting.

Models of both the small and large probes were constructed in order to make free air drops from a helicopter which would simulate the conditions of Mach number and Reynolds number to be encountered by the probes upon entry into the Venus atmosphere. The drops were conducted at the U.S. Army tank gunnery range at Ft. Riley, Kansas. The probes were released from an Air National Guard helicopter at an indicated altitude of 3,046 M(10,000 ft.) MSL. The altitude of the impact area was 408 M (1340 ft.) MSL.

Of specific interest during these tests were:

a. The magnitude and signatures of the aerodynamic buffeting under quiescent air conditions at a Reynolds number of approximately 3×10^6 and a Mach number of about .1.

b. The aerodynamic and dynamic behavior in free flight.

c. The drop velocities and vertical flow velocities of the atmosphere from on board measurements.

d. A test of the temperature and pressure sensors.

e. The determination of the lift and drag coefficients from accelerometer records .

f. A definition of the probe angles of attack and side slip from accelerometer records.

2. PROBE MODELS AND PROCEDURE

2.1 Models

The complete models of the small and large probes are shown in Figures 2.1.1 and 2.1.2 at the Flight Research Laboratory prior to departure for the drop site. Sketches of the models with key dimensions are given in Figures 2.1.3 and 2.1.4.

The models were constructed in two sections. The forty-five degree nose cone of the small probe and the portion of the large probe forward of the separation ring were molded from 6.35 mm plastic. The inside of each was filled with foam with the instrumentation package, batteries and balance weights placed in the foam as shown in Figure 2.1.5. The rear sections were bolted to the forward sections and contained a lift hook on the centerline of the model. On the small probe two foam filled boxes were attached to the outer portion of the rear hemisphere to simulate the probe instrumentation packages. On the large probe vanes were attached to the separation ring, and the instrumentation packages just aft of the separation ring were simulated.

The complete models were weighed and balanced in the laboratory, Table I. The model probes were painted yellow and the x, y and z accelerometer axes were marked on the outside of the models with black tape.

2.2 Instrumentation

The probe model instrumentation package, Figures 2.2.1 and 2.2.2, consisted of the following elements:

1. Three accelerometers for sensing the accelerations along the x, y, and z body axes.
2. One pressure transducer to measure total pressure.
3. One thermistor to measure ambient temperatures.
4. A photo cell to record rate of spin.
5. Signal conditioning and telemetry down link transmitter.

The recording instrumentation at the drop site consisted of an antenna, receiver, magnetic tape recorder and a strip chart recorder, Figure 2.2.3.

The indicated altitude of the helicopter was recorded from the pilot's altimeter. The pressure altitude of the helicopter was recorded from the co-pilot's altimeter. In addition a third altimeter was carried to record pressure altitude. The temperature was recorded from the pilot's outside air temperature gage. A motion picture camera was taken aloft in the helicopter to photograph the initial phase of the flights. A transit was used at the ground station to position the helicopter over the probe model drop point.

2.3 Drop procedure

The drops were conducted at the tank gunnery range at Fort Riley, Kansas, at dawn on 15 June, 1977, (small probe) and 3 August, 1977, (large probe). The probe instrumentation and ground receiving equipment was tested and calibrated in the laboratory the morning before the

drop date. The model was transported to the drop site in the afternoon, and the equipment was set up on site during the evening (after the tank range firing was completed). The model and recording instrumentation was again tested and the calibration checked on site.

The Kansas Air National Guard helicopter from Forbes Field, Topeka, Kansas, arrived at the drop site just before dawn. The model was attached to the helicopter at the site, Figure 2.3.1. The probe instrumentation and recording equipment were then checked with the helicopter in hovering position and the model attached. The helicopter than proceeded to climb to an indicated altitude of 3046 M (10,000 ft.) MSL. During the climb periodic recordings were made of the data from the probe sensors. Each 152 M (500 ft.) during the climb readings were taken of the three altimeters and the outside temperature gauge in the helicopter. When an altitude of 3046 meters was reached, the helicopter approached the drop point and dropped the probe on signal from the transit observer. A continuous recording of the probe sensors was made during the drop. Motion pictures of the drop were made from the helicopter, Figures 2.3.2 and 2.3.3.

Following the drop, photographs were made of the model at the drop site, Figures 2.3.5, 2.3.6, and 2.3.7. The instrumentation package was salvaged and returned to the laboratory.

3. RESULTS

3.1 Small Probe Model

The small probe model was continuously observed from the helicopter and the ground during its flight. The model was not observed to rotate. Motion pictures from the helicopter and the on-board sensor confirmed this observation.

The small probe model was observed to pitch very briefly shortly after release. This rapidly damped out, and the probe descended in a very stable manner with no motion visibly observed.

The initial two seconds of the transmissions from the probe after drop were masked by static. The data during this period were reconstructed from the motion picture record. Two other times during the flight static electricity apparently built up on the model and masked the signal. Except for these brief periods all six channels functioned properly.

The x, y, and z body axes accelerometer records and the temperature and pressure records which were telemetered from the probe to the ground were digitized. The z wind axis accelerations were obtained from the digitized x, y, and z body axes valves. The z wind axis accelerations were then integrated to obtain the velocities and altitudes of the probe during its flight. The base level of the z wind axis accelerations was corrected to make the final integrations agree with the drop distance and the average flight velocity. Figure 3.1.1 is a plot of the instantaneous velocities during the flight. Probe altitude during the flight is shown in Figure 3.1.2. The accuracy of the drop distance determined from the helicopter instrumentation was ± 53 meters. The accuracy of the measured drop time was ± 1 second. The average velocity during the flight computed from the drop distance and drop time was 34.3 ± 1 meters per second.

The velocities of the probe during flight were also obtained from the rate of change of the total pressure measured during flight, Figure 3.1.3. Relatively wide intervals of time had to be selected to determine the slope of the recorded pressure trace. Because the rate of pressure

change was small, the accuracy of the velocities calculated from the pressure data is considered to be less than those calculated from the accelerometer data.

The coefficients of drag (z wind axis), Figure 3.1.4, were calculated from the following:

1. Flight velocities which were obtained from the integration of the corrected z wind axis accelerations.
2. Cross-section area of the probe at the separation point.
3. Air densities which were calculated from the pressure and temperature profiles measured by the instrumentation in the helicopter during the climb from the drop site to the drop altitude.
4. Drag force which was assumed to be equal to the weight of the probe.

The average drag coefficient, C_D=.714, was calculated by an integration of the local coefficients over the flight distance. During the first three seconds after the release of the probe from the helicopter, the probe was accelerating in speed and the calculated coefficients of drag decreased rapidly. The probe was in some downwash during this period and oscillating in sideslip, β . From about the four-second mark onward the probe was stable and the calculated coefficients of drag remained relatively constant until the last twenty seconds of flight. There appeared to be no explanation for this increase in the drag coefficients during the later period unless there was a small updraft at the lower altitudes near the ground. The basic velocity profiles, Figures 3.1.1 and 3.1.3, were very similar in shape and magnitude. The density varied smoothly and nearly linearly with altitude.

The Reynolds numbers varied from 2.95×10^6 to 2.50×10^6 during the flight. The average Reynolds number was 2.84×10^6. The corresponding average drag coefficient of .714 compared with the wind tunnel

drag coefficient of .812 at a Reynolds number of 7.02×10^5, Figure 3.1.5. All valves were based upon the maximum diameter of the probe and corresponding area. The decrease in the drag coefficient of .098 units from the wind tunnel value may have been a result of any or all of the following:

1. Small motion of the probe in free flight.
2. Modeling differences.
3. Wind tunnel corrections.
4. Reynolds number effect.
5. Experimental error.

The wind tunnel data indicated that motion of the probe decreased the coefficient. However, the small motion of the probe in flight should not have had much effect. The chief difference in modeling occurred by the addition of the two box-like instrumentation packages on the free flight model. The position of these behind the separation point should decrease the drag.[3,4] The wind tunnel corrections were small in themselves, and the error in the corrections should not have been significant. The effect of Reynolds number is not known, although in the various tunnel tests at lower Reynolds numbers the coefficient increased slightly with increasing Reynolds number.[1] The accuracy of the wind tunnel data was ± 3%. The accuracy of the drop data was about ± 6%. It would appear that the lower coefficient of drag from the drop test was valid and was most nearly representative of the actual small probe entry conditions to Venus.

The coefficients of lift (wind axes) were obtained as a function of time from the wind tunnel lift/side force coefficients using the resultant relative wind angle, $\bar{\alpha} + \bar{\beta}$ (total angle between the relative wind vector and the z axis of the probe). The lift coefficients are

shown in Figure 3.1.6; the wind tunnel lift coefficients, in Figure 3.1.7.

The angles of attack (α) about the y axis and the sideslip angle (β) about the x axis were determined from the x and y body axes accelerometer data and the wind tunnel data as it varied with angle of attack/yaw. It was assumed that the probe models were symmetrical about the z body axis.

Since

$$a_{x,y} = \sin \alpha,\beta - \frac{C_{S_{F_{x,y}}}}{C_{D_w}} \qquad \text{and} \qquad \frac{C_{S_{F_{x,y}}}}{C_{D_w}} = f(\alpha,\beta)$$

$$\beta,\alpha = f\left(a_{x,y} \;\&\; \frac{C_{S_{F_{x,y}}}}{C_{D_w}}\right)$$

where $a_{x,y}$ were measured by the probe and $\frac{C_{S_{F_{x,y}}}}{C_{D_w}}$ are known from the wind tunnel data as a function of α,β. α, β were determined by successive approximations as functions of $a_{x,y}$. The calculated angles of attack (α) and sideslip (β) are plotted in Figures 3.1.8, 3.1.9, 3.1.10 and 3.1.11.

The total angle between the relative wind vector and the z axis of the probe ($\bar{\alpha} + \bar{\beta}$) was calculated. The directions of the resultants from the x axis are plotted in Figures 3.1.12 and 3.1.13. The absolute magnitudes of the resultants are plotted in Figures 3.1.14 and 3.1.15. Plots were made of the motion of the angles of attack (α) and sideslip (β) in a plane perpendicular to the z axis for each second during flight. Figures 3.1.16 through 3.1.18 are representative of these p'ots.

The visual observations made during the small probe model flight, the motion picture records and the calculations made from the data obtained from the on board sensors indicate:

1. The model was very stable in flight.
2. The model did not rotate.
3. The large oscillation in sideslip (9.1 degrees) induced in launch damped to half amplitude within 4 seconds after launch.

4. After the large launching oscillations were damped out, the maximum values of angle of attack and sideslip were 3.2 and 4.0 degrees, respectively. Generally values of both were below 2 degrees.

5. After the large launching oscillations were damped out, the maximum value of the resultant of the angle of attack and sideslip was 4.15 degrees. Generally values were under 2 degrees.

6. The angle of attack about the y axis oscillated at three frequencies, 2.9, .53 and .14 cycles per second. The angle of sideslip about the x axis oscillated at frequencies of 2.9, .47 and .05 cycles per second, Table II.

7. The resultant of the angle of attack and sideslip oscillated at frequencies of 3.1, .31 and .05 cycles per second.

8. A plot of the small motion of the probe in angle of attack and sideslip in a plane perpendicular to the z axis was random in nature.

9. The drag coefficient calculated from the accelerometer data increased as the model approached the ground. The model was under the influence of a vertical air flow which shifted from downward at launch to upward approaching the ground.

10. The average drag coefficient was .714. The average Reynolds number was 2.84×10^6, and the average Mach number was .10.

11. The maximum lift coefficient was .025 with values generally less than .01.

3.2 Large Probe Model

The large probe model was continuously observed from the helicopter and the ground during its flight. The model was observed to rotate slowly. The motion picture frames indicated that the model commenced rotating immediately after launch. The rotation built up momentarily to a rate of about 17 r.p.m. in 2.5 seconds. By three seconds the rotation rate steadied at about 5 r.p.m. The signal of the on board sensor for rotation did not record properly. Likewise, the pressure and temperature channels did not function properly. The x, y and z accelerometer functioned properly, and the data were recorded.

The model was visually observed to pitch and yaw excessively after launch. Although this damped out some, the pitching and yawing were visually observed throughout the flight. The motion pictures and the values of angle of attack and sideslip calculated from the accelerometer data confirmed the pitching and yawing of the model.

The accelerometer records were digitized. From the integration of the corrected accelerometer data, the velocity of the probe model and its altitude were obtained, Figures 3.2.1 and 3.2.2. The coefficients of drag were calculated from the velocity data and are plotted in Figure 3.2.3 for the flight. The average coefficient of drag from Figure 3.2.3 was .663 at an average Reynolds number of 2.90×10^6. The wind tunnel drag coefficients for various angles of attack/sideslip are plotted in Figure 3.2.4 for a Reynolds number of 8.58×10^5. The values range from .825 for zero degrees sideslip to .695 for 30 degrees sideslip. All data were based upon the maximum diameter of the separation ring. The decrease in the drop test drag coefficient is considered to be primarily the result of:

1. The inflight motion of the probe.
2. Smoother surface of the drop test probe.
3. Possibly Reynolds number.

The coefficients of lift were calculated from the accelerometer data and are shown in Figure 3.2.4. Using the wind tunnel data of lift coefficient, Figure 3.2.6, and the accelerometer data, the angles of attack and sideslip were calculated and are plotted in Figures 3.2.7, 3.2.8, 3.2.9, and 3.2.10. The resultants of the angles of attack and sideslip were calculated. The directions of the resultants from the x axis are plotted in Figures 3.2.11 and 3.2.12. The absolute magnitudes of the resultants are plotted in Figures 3.2.13 and 3.2.14. Plots of angles of attack (α) and sideslip (β) for each

second during flight were made. Figures 3.2.15 through 3.2.17 are representatives of these plots. The plots indicate that the resultant rotated at a rate of 1.1 cycles per second and that the mean during the cycle was not at zero. This may be the result of the "Knuckle ball" effect, an offset of the center of gravity from the z axis and/or the probe not being symmetrical about the z axis which produced unsymmetrical aerodynamic forces. In wind tunnel tests[1] the large probe displayed a subdued "Knuckle ball" effect as compared to a sphere. The probe was suspended from the ceiling in the laboratory along the x, y and z axes to position the center of gravity. The error in its position should be negligible. The cloud particle sensor made the probe unsymmetrical about the z axis.

The visual observations made during the large probe model flight, the motion picture records and the calculations made from data obtained from the on board sensors indicated:

1. The model was stable in flight.
2. The model rotated at about 5 r.p.m.
3. The large oscillations in angles of attack (26.5 degrees) and in sideslip (30.0 degrees) after launch damped to half amplitude in 25 and 20 seconds, respectively, after launch.
4. After the large launching oscillations were damped out, the angles of attack and sideslip oscillations were generally under 10°.
5. The maximum resultant of angles of attack and sideslip (33 degrees) was damped to half amplitude in 32 seconds after release.
6. After the large launching oscillations were damped out, the resultant of angles of attack and sideslip oscillations were generally under 13 degrees.
7. The angle of attack about the y axis and the angle of sideslip about the x axis oscillated at two frequencies, 1.1 and .14 cycles per second, which were superimposed on the rotational motion of about the .08 r.p.s., Table II.

8. The resultant of the angle of attack and sideslip oscillated at two frequencies, 1.1 and .14 cycles per second.

9. A plot of the motion of the probe in angle of attack and sideslip in a plane perpendicular to the z axis indicated that the resultant rotated at a rate of 1.1 cycles per second.

10. The average drag coefficient was .663 at an average Reynolds number of 2.90×10^6 and an average Mach number of .10.

11. The maximum lift coefficient was .48 with values generally less than .20.

4. CONCLUSIONS

Large amplitude motions were induced in the launching of both probes. The motion of the small probe after launch damped more rapidly than did that of the large probe. The continued oscillations of the small probe were about one-fifth the amplitude of the large probe. Both probes exhibited oscillations in angle of attack and sideslip at distinct frequencies. The motion of the small probe in a plane perpendicular to the z axis was random in nature but the large probe rotated (corkscrewed) about the z axis at 1.1 cycles per second.

The average drag coefficient of the small probe was .714 at a Reynolds number of 2.84×10^6 and a Mach number of .10. The average drag coefficient of the large probe was .663 at a Reynolds number of 2.90×10^6 and a Mach number of .10.

5. REFERENCES

1. Muirhead, Vincent U., "Investigation of the Probe Buffeting Problem at Low Subsonic Mach Numbers," Flight Research Laboratory Report FRL 500, University of Kansas, July, 1975.

2. Sorensen, T.C. and Muirhead, V.U. "Wind Tunnel Investigation of Low-Speed Buffeting of the Pioneer Venus Probes," Journal of Spacecraft and Rockets, Jan/Feb 1978, pp. 34-39.

3. Muirhead, Vincent U., "An Investigation of Drag Reduction on Box-Shaped Ground Vehicles," KU-FRL 180, July, 1976.

4. Muirhead, Vincent U., "An Investigation of Drag Reduction for Tractor Trailer Vehicles," KU-FRL 332-1, October 1977.

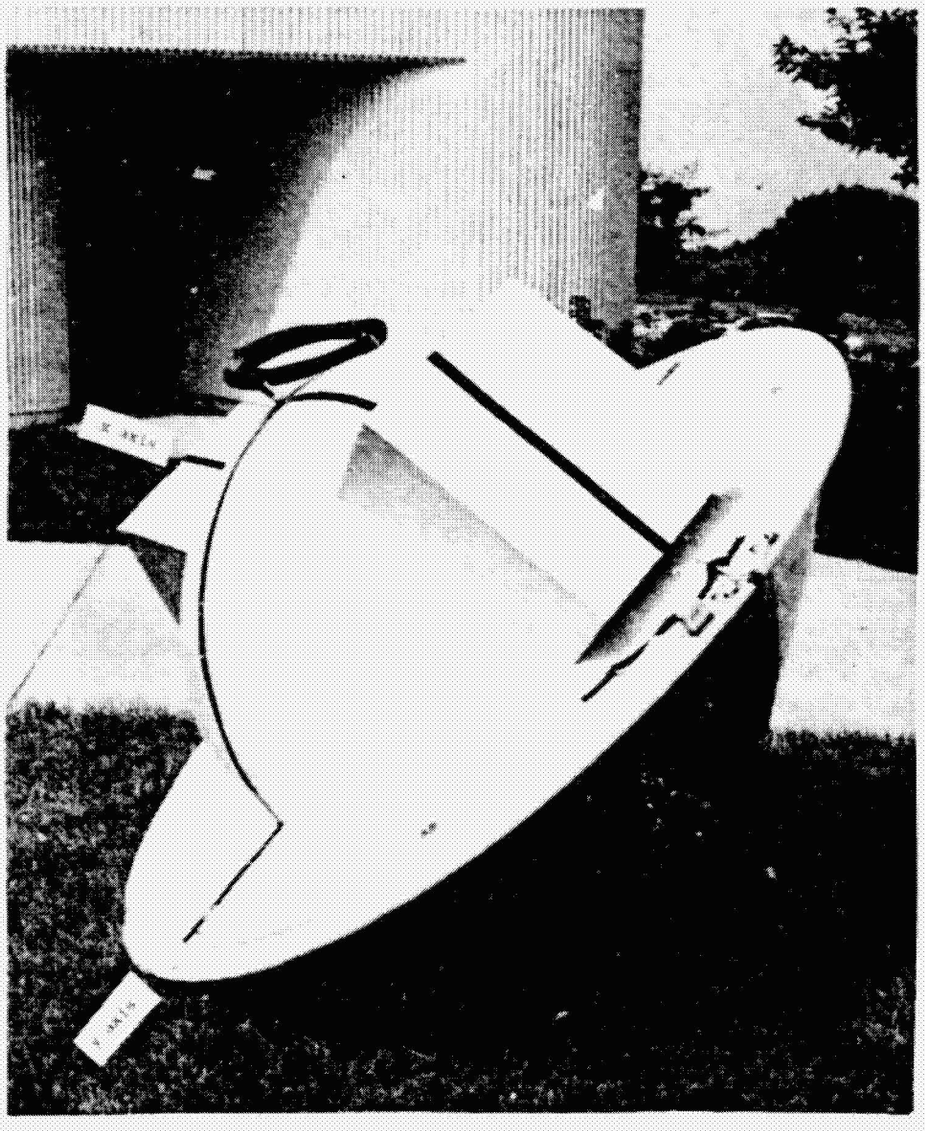

Figure 2.1.1 Assembled small probe model.

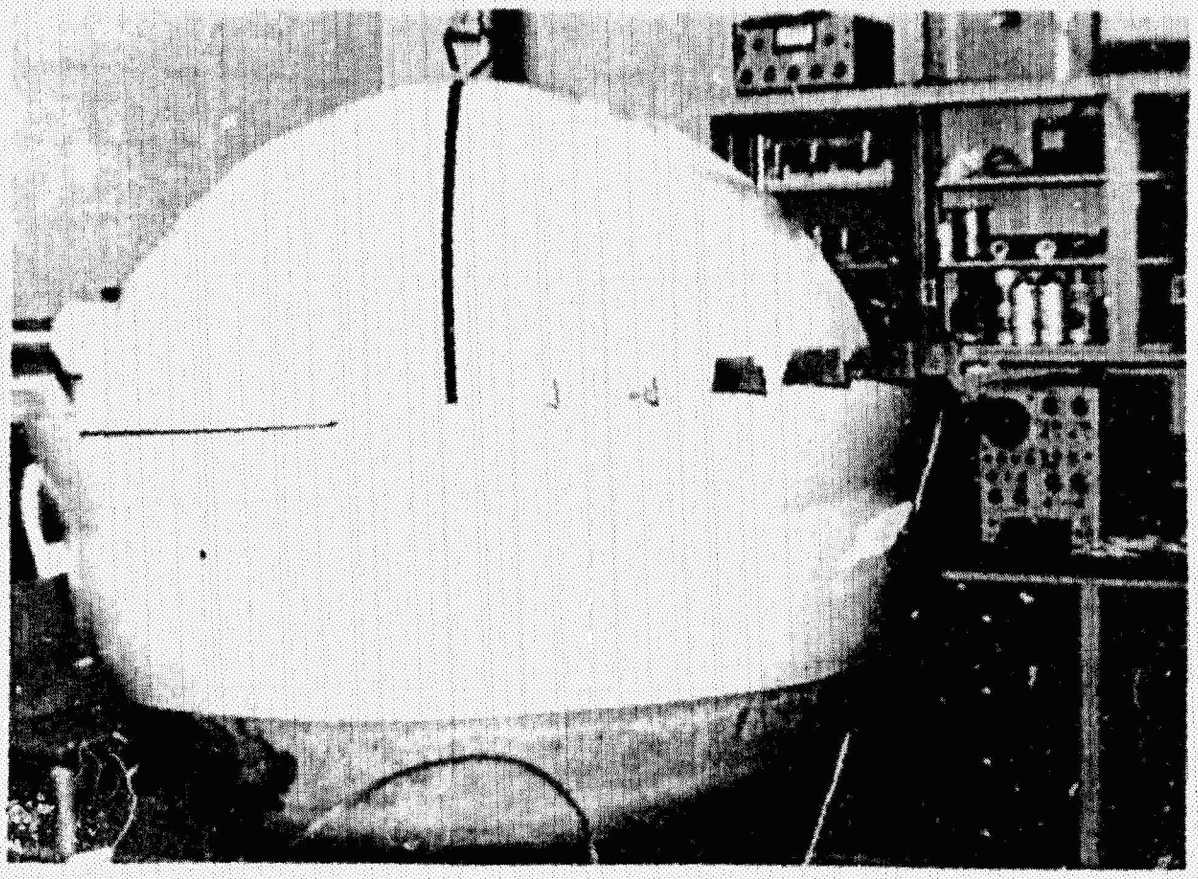

Figure 2.1.2 Assembled large probe model.

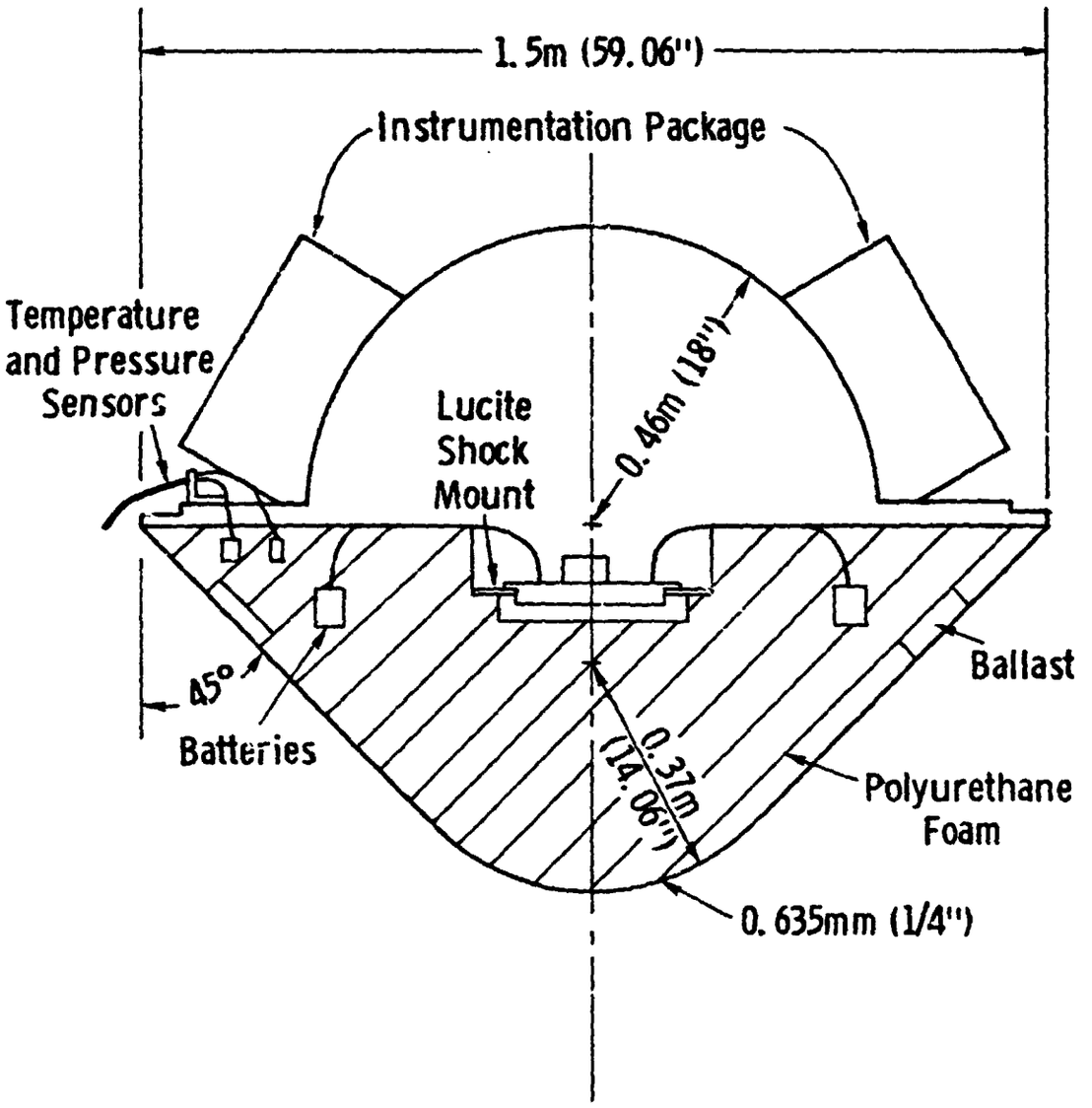

Figure 2.1.3. Small Probe Assembly Sketch.

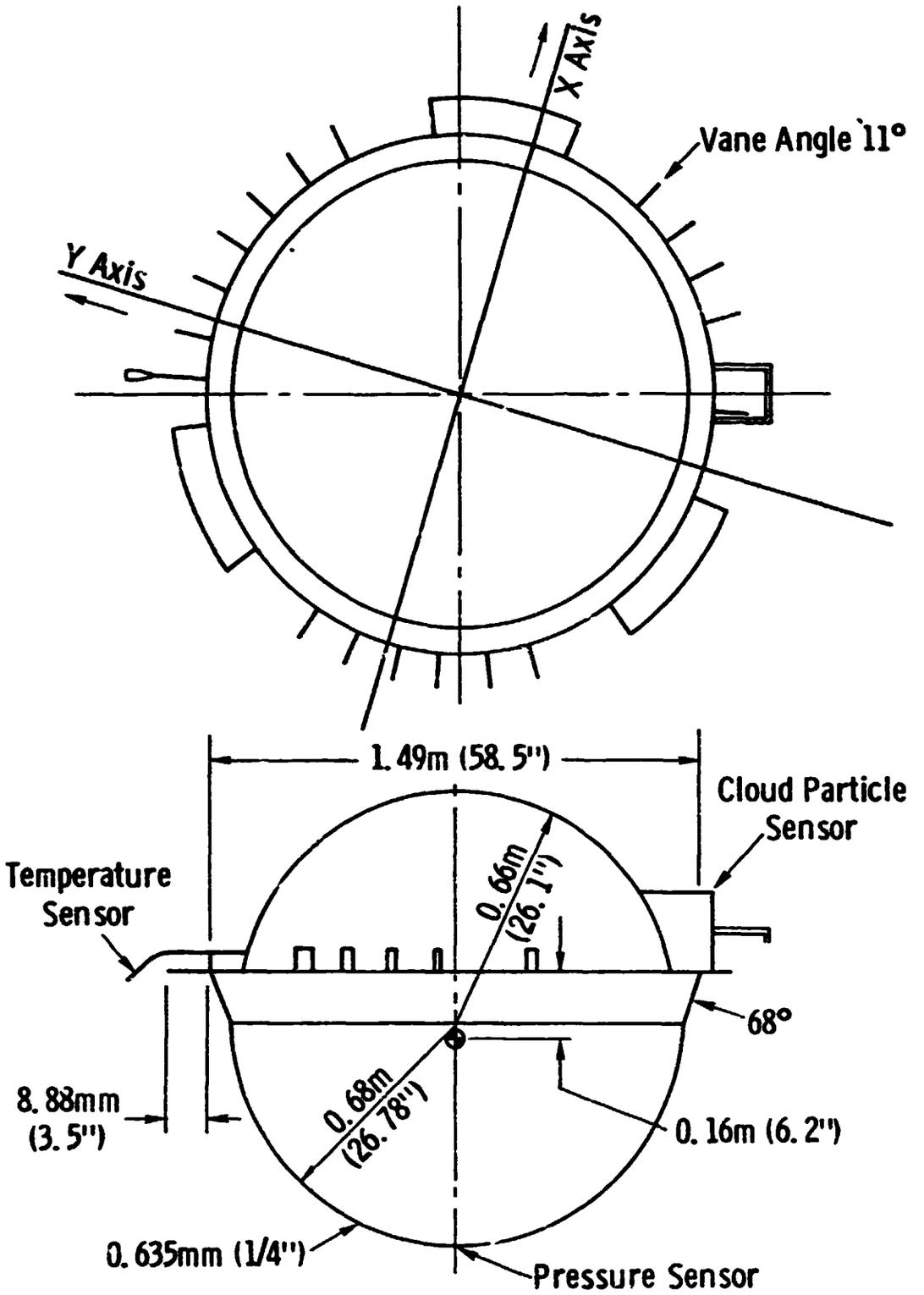

Figure 2.1.4. Large Probe Assembly Sketch.

Figure 2.2.1 Small probe sensors and telemetry.

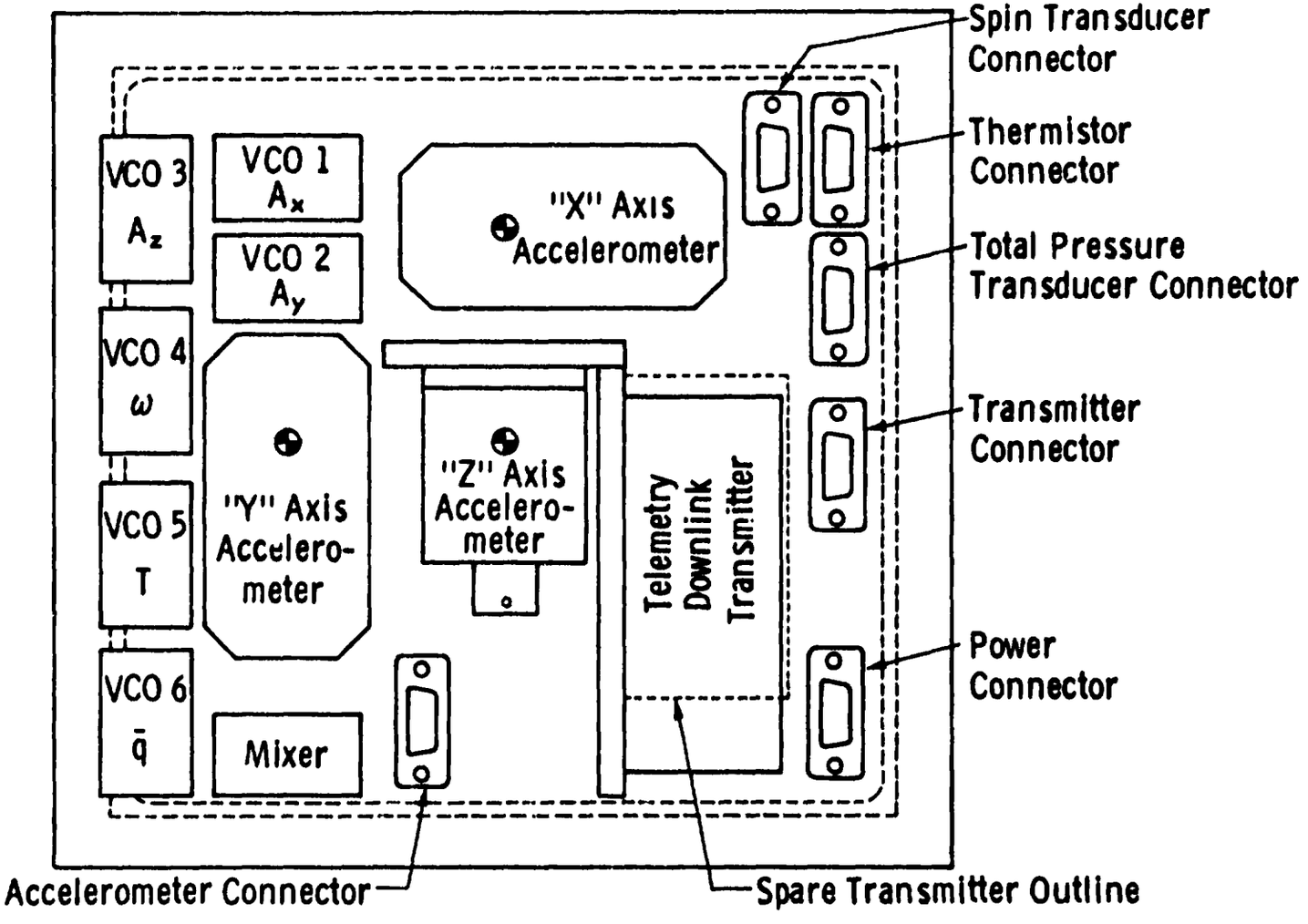

Figure 2.2.2. Instrumentation Package

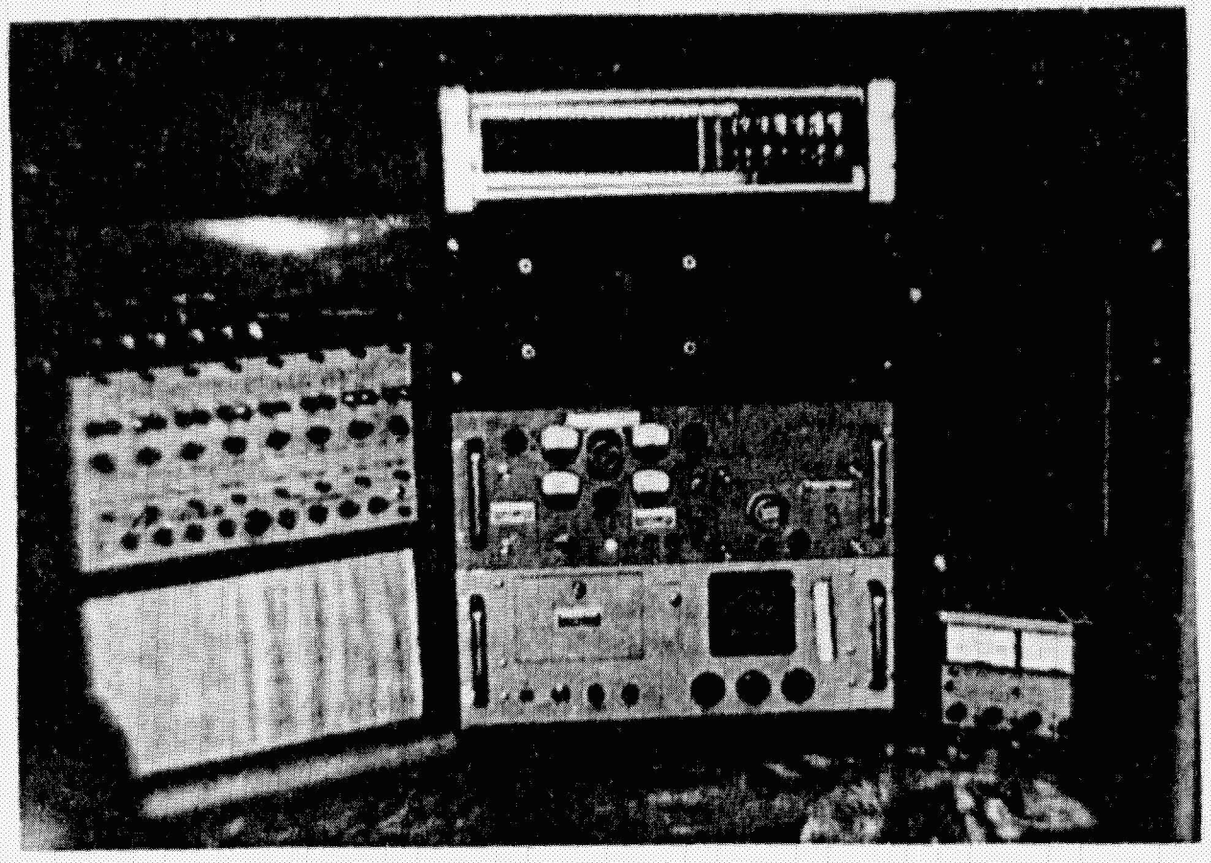

Figure 2.2.3 Ground Recording equipment.

Figure 2.3.1 Large probe model being attached to helicopter.

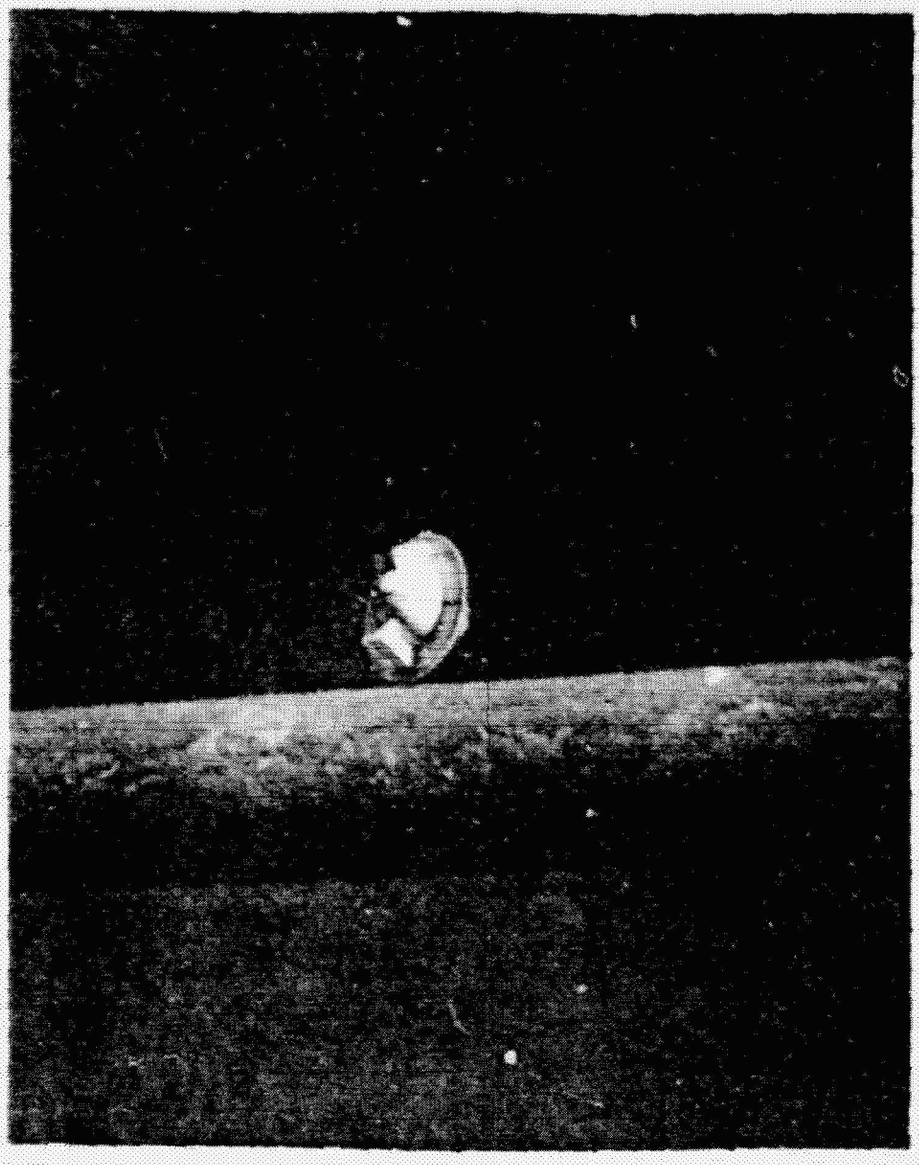

Figure 2.3.2 Small probe model in flight.

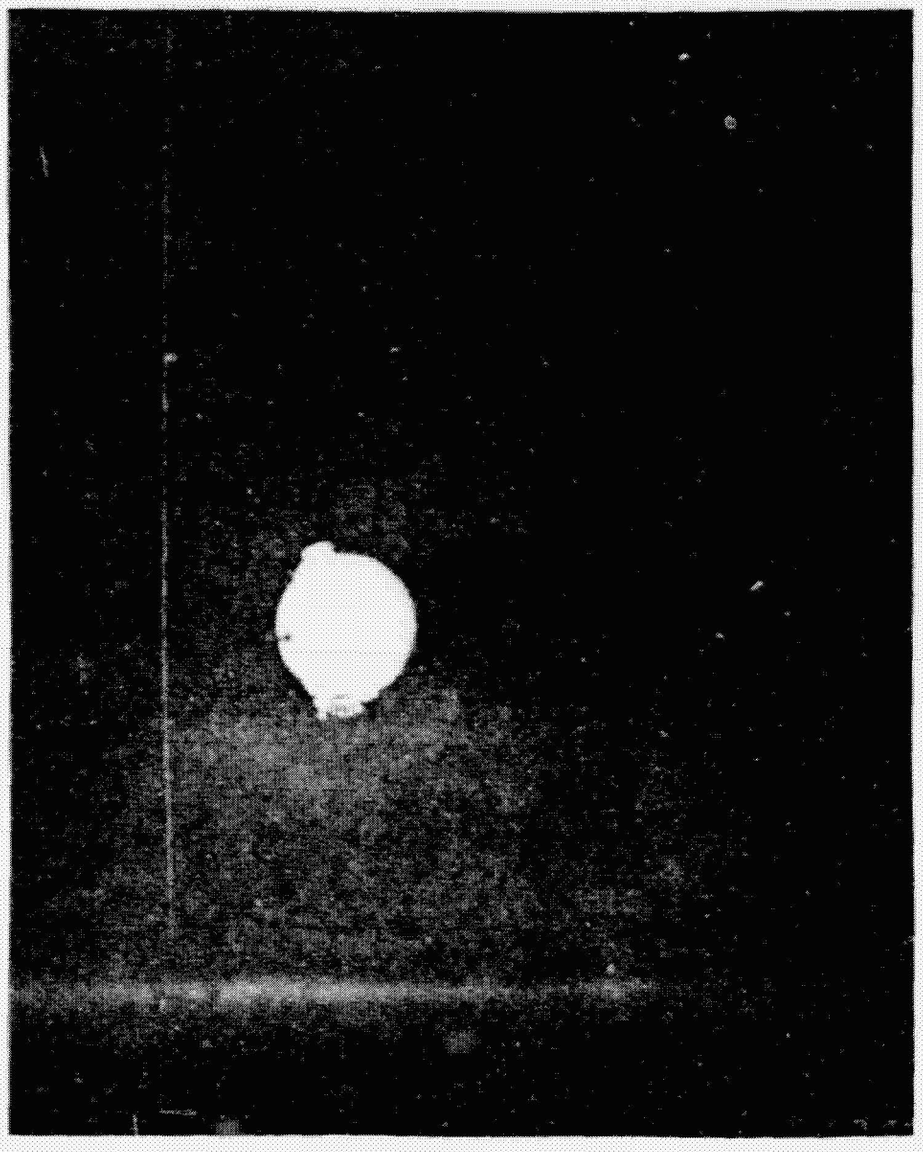

Figure 2.3.3 Large probe model in flight.

Figure 3.3.4 Small probe after impact.

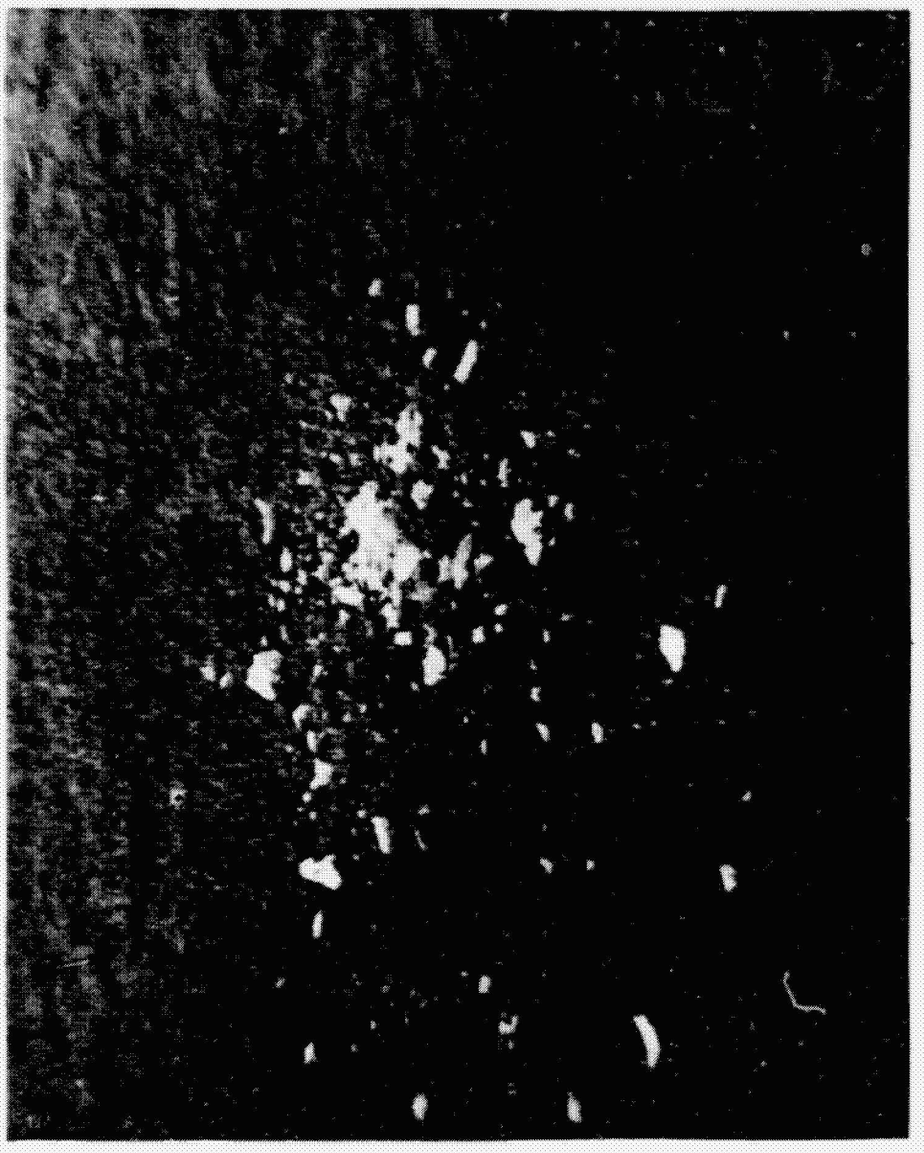

Figure 2.3.5 Large probe impact area.

Figure 2.3.6 Large probe instrumentation package after impact.

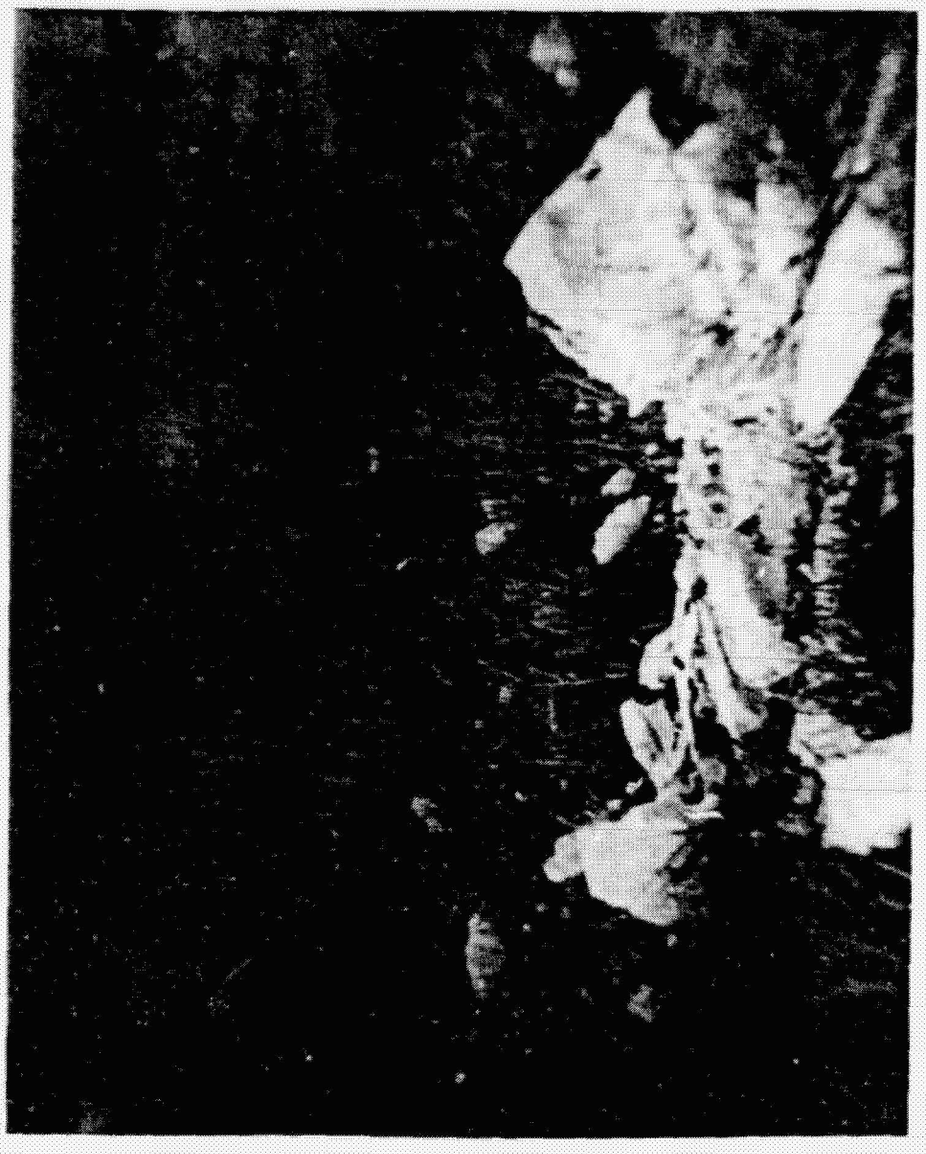

Figure 2.3.7 Large probe parts after impact.

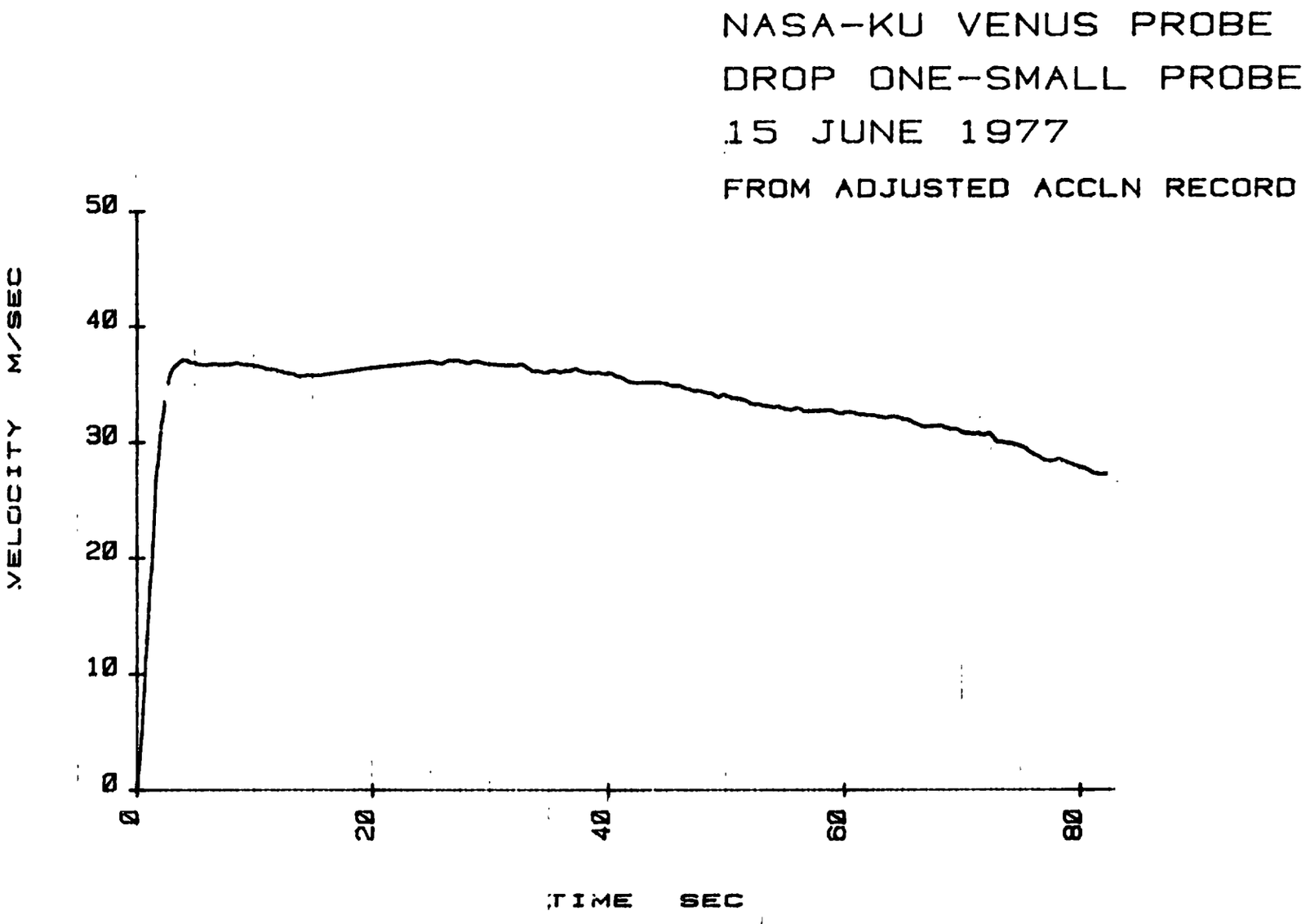

Figure 3.1.1 Small probe velocity from accelerometer data.

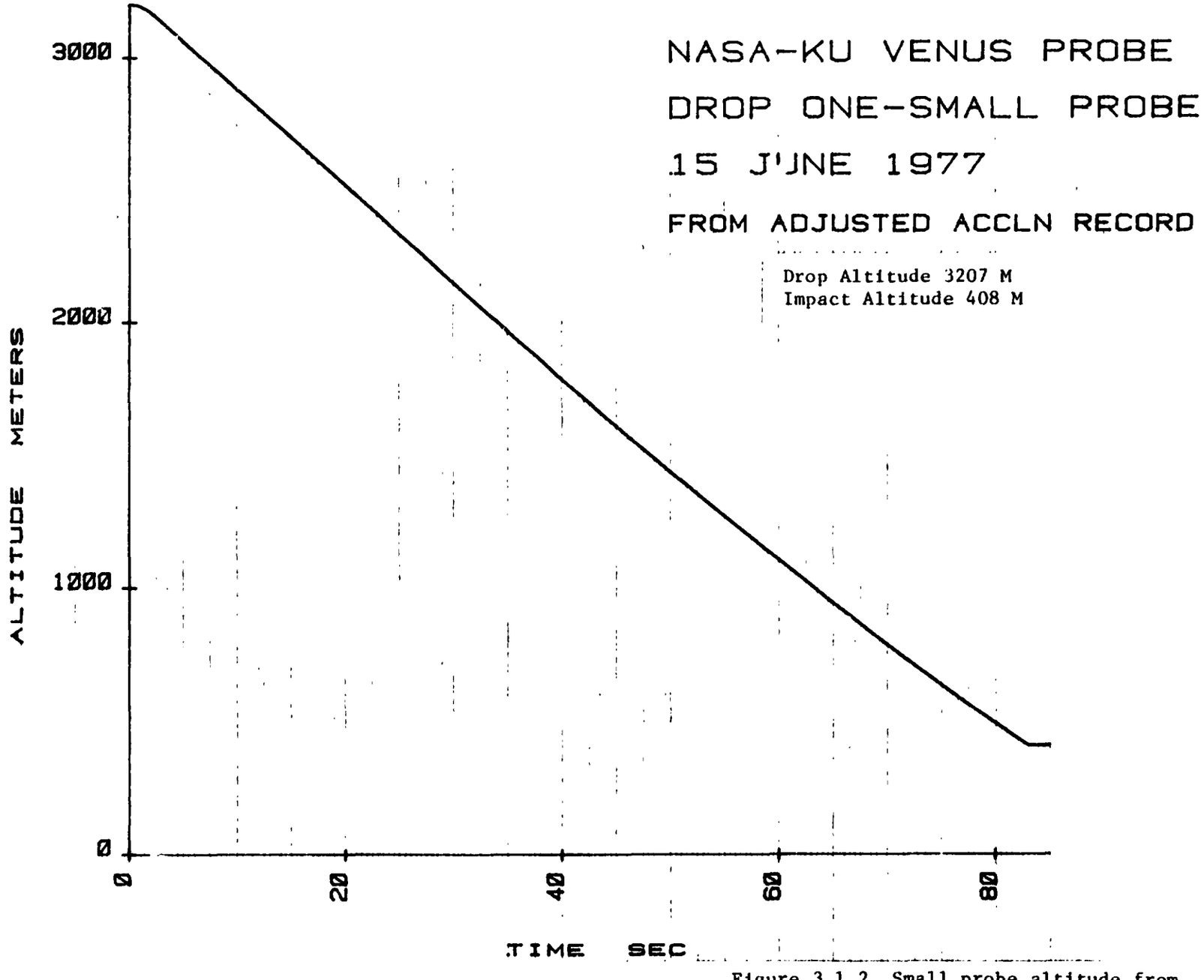

Figure 3.1.2 Small probe altitude from accelerometer data.

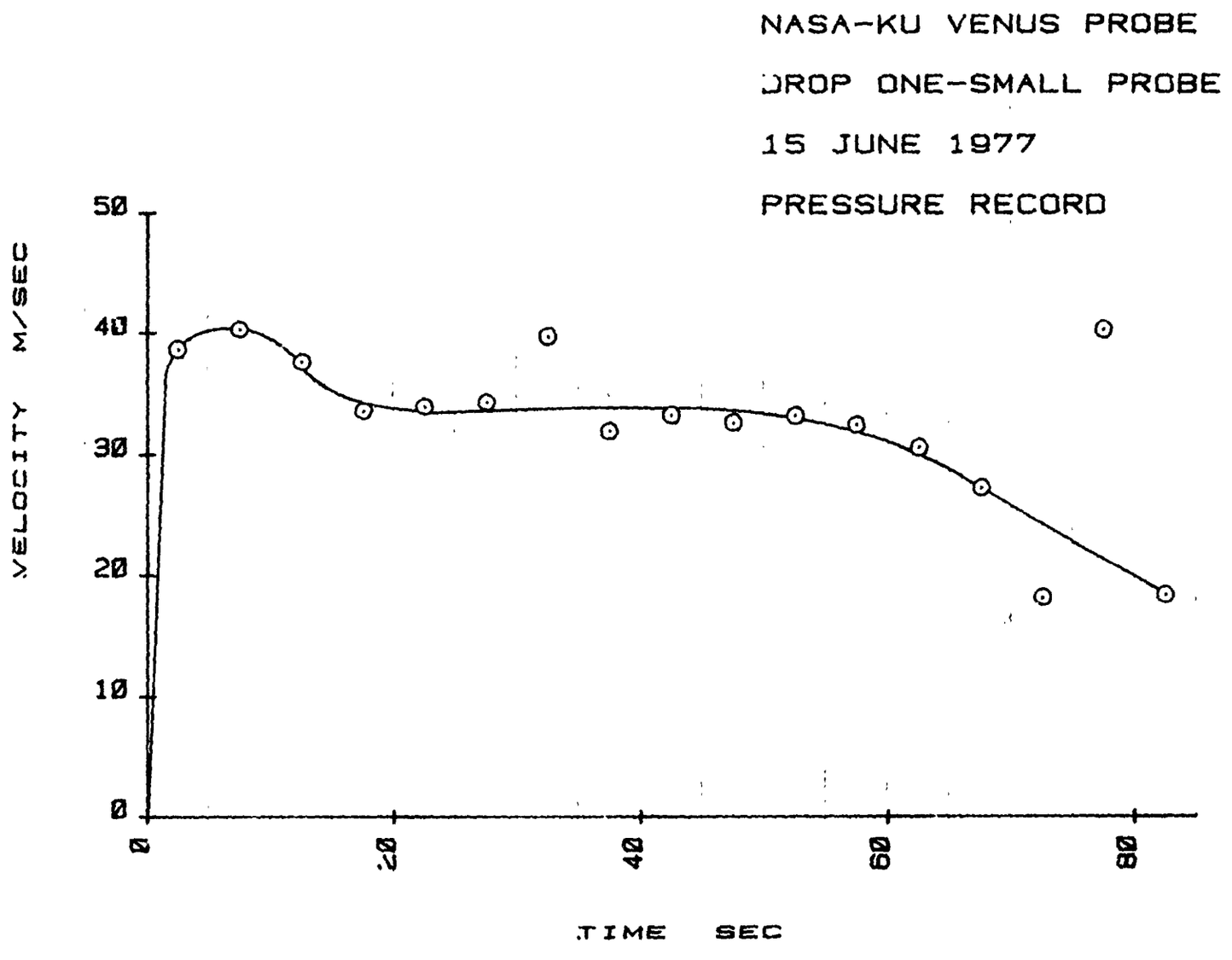

Figure 3.1.3 Small probe velocity from pressure data.

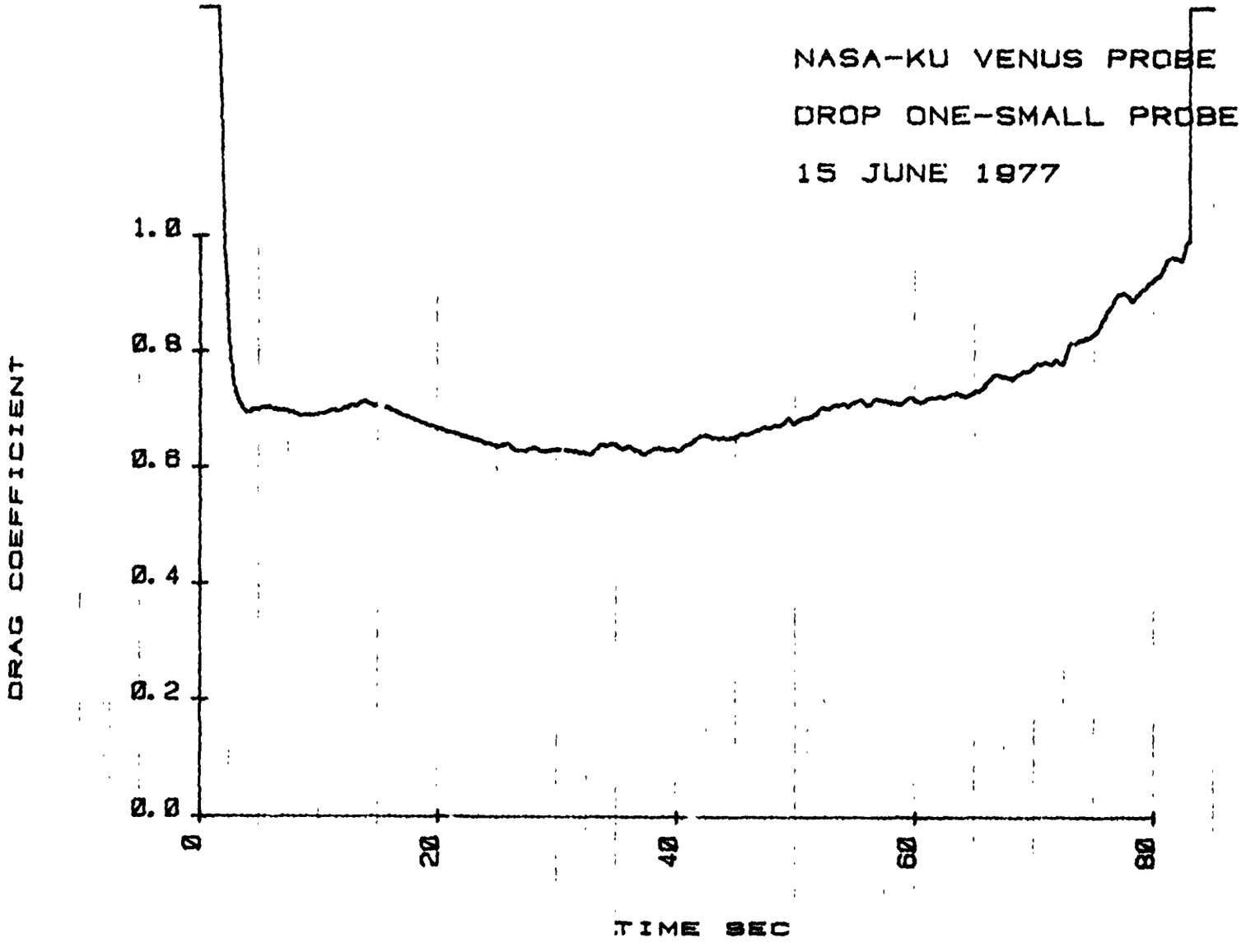

Figure 3.1.4 Small probe drag coefficient from accelerometer data.

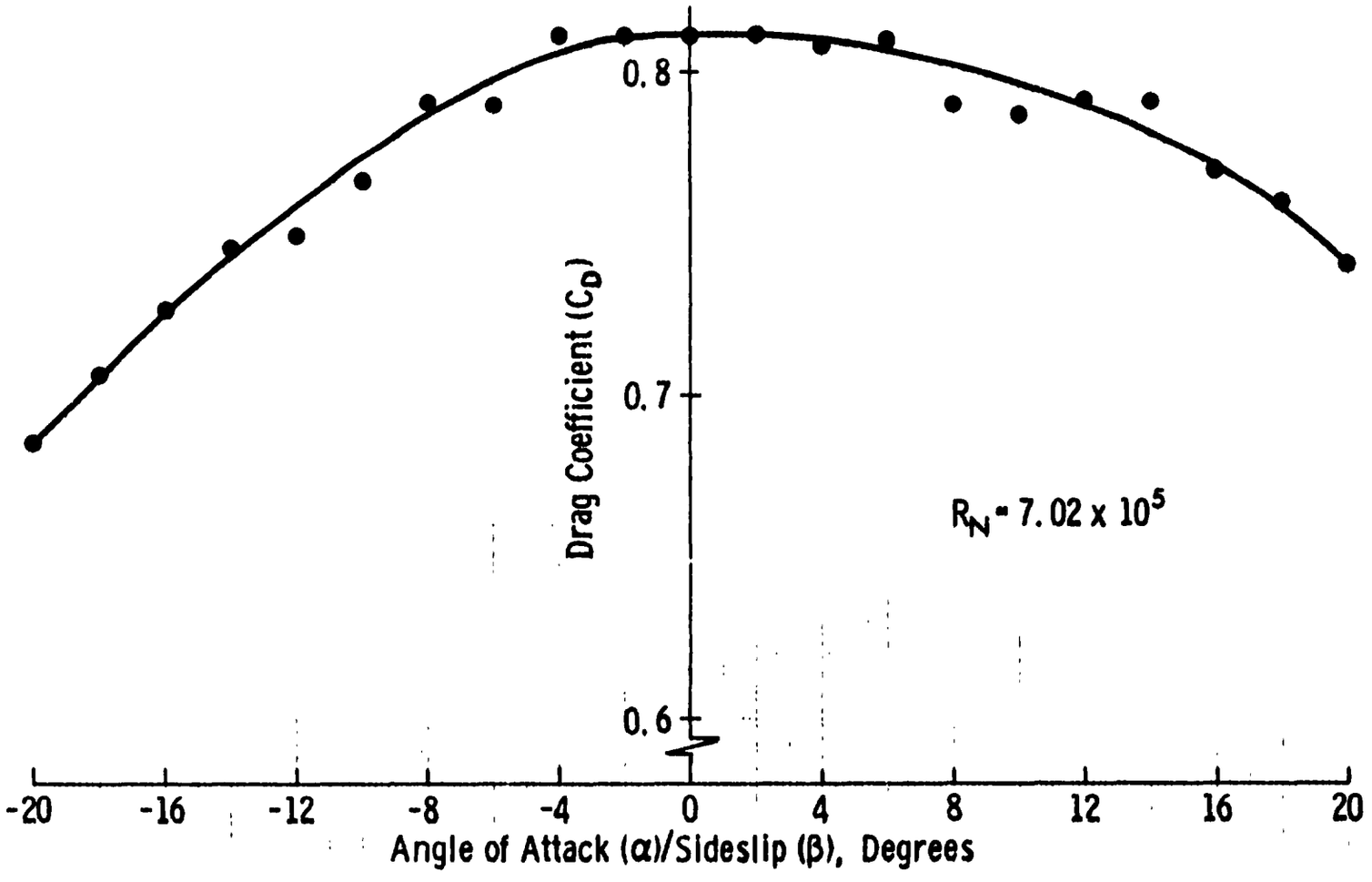

Figure 3.1 5. Small Probe Drag Coefficient from Wind Tunnel Data.

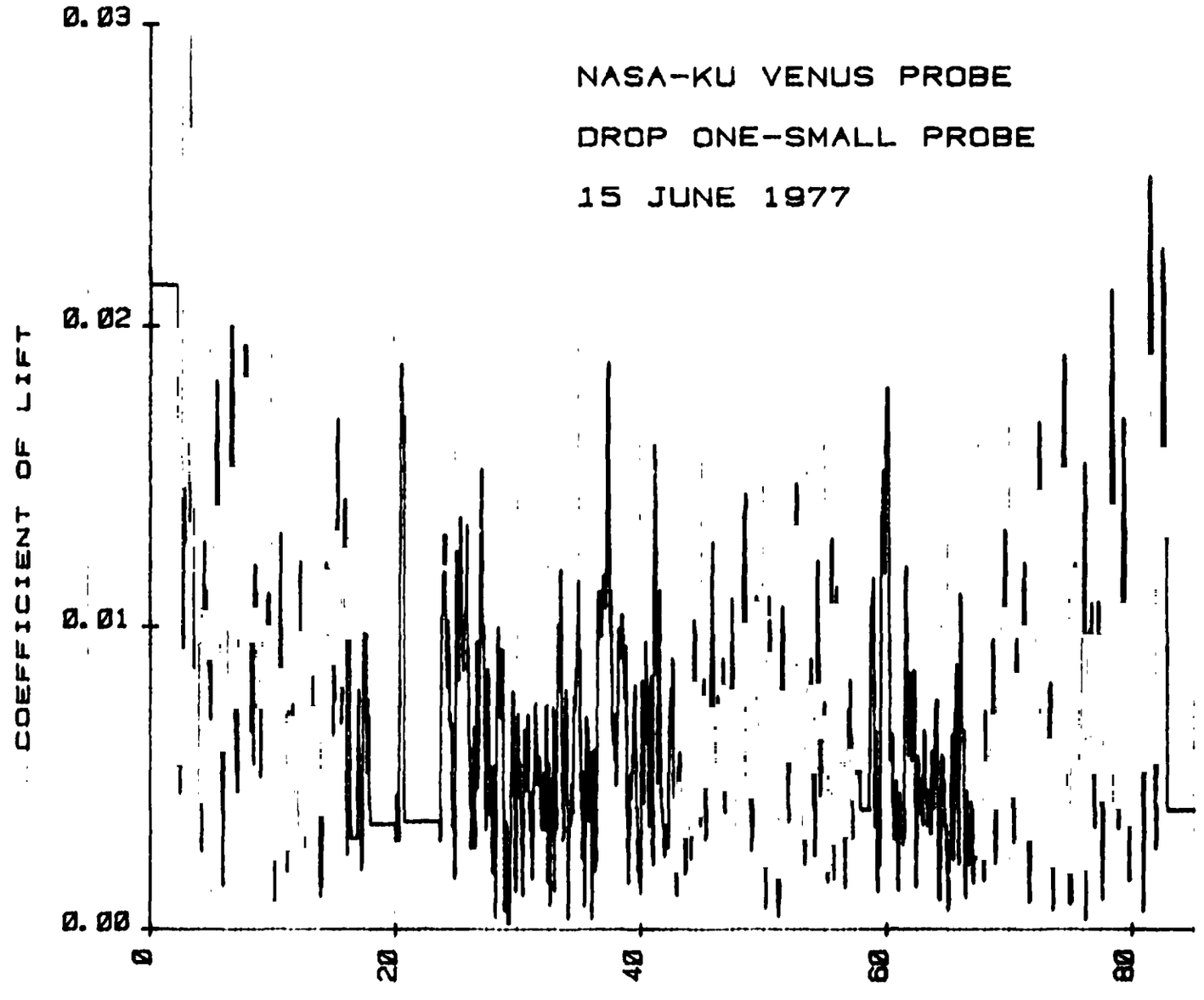

Figure 3.1.6 Small probe lift coefficient (resultant of lift and side force).

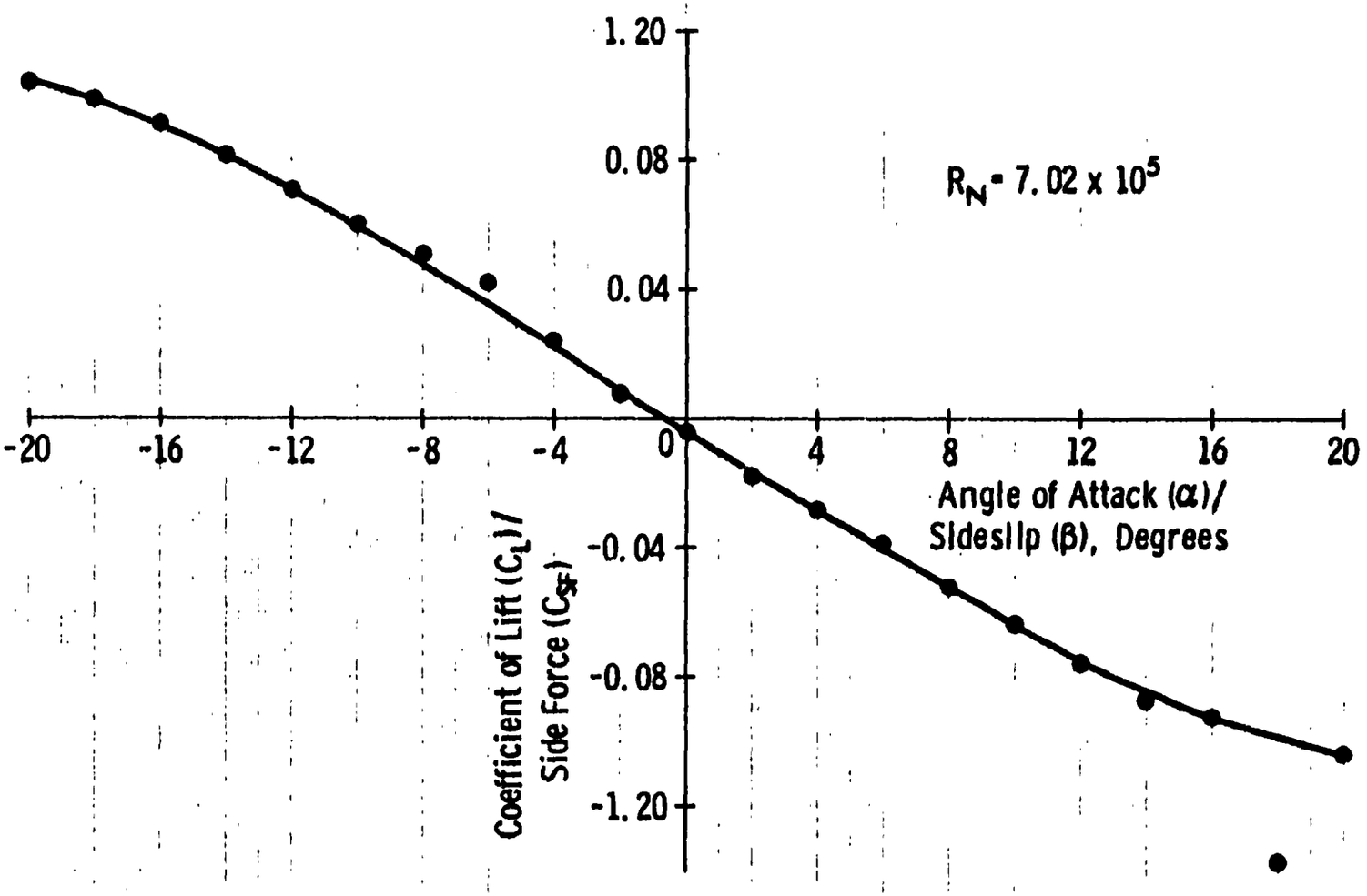

Figure 3.1.7. Small Probe Lift Coefficient from Wind Tunnel Data.

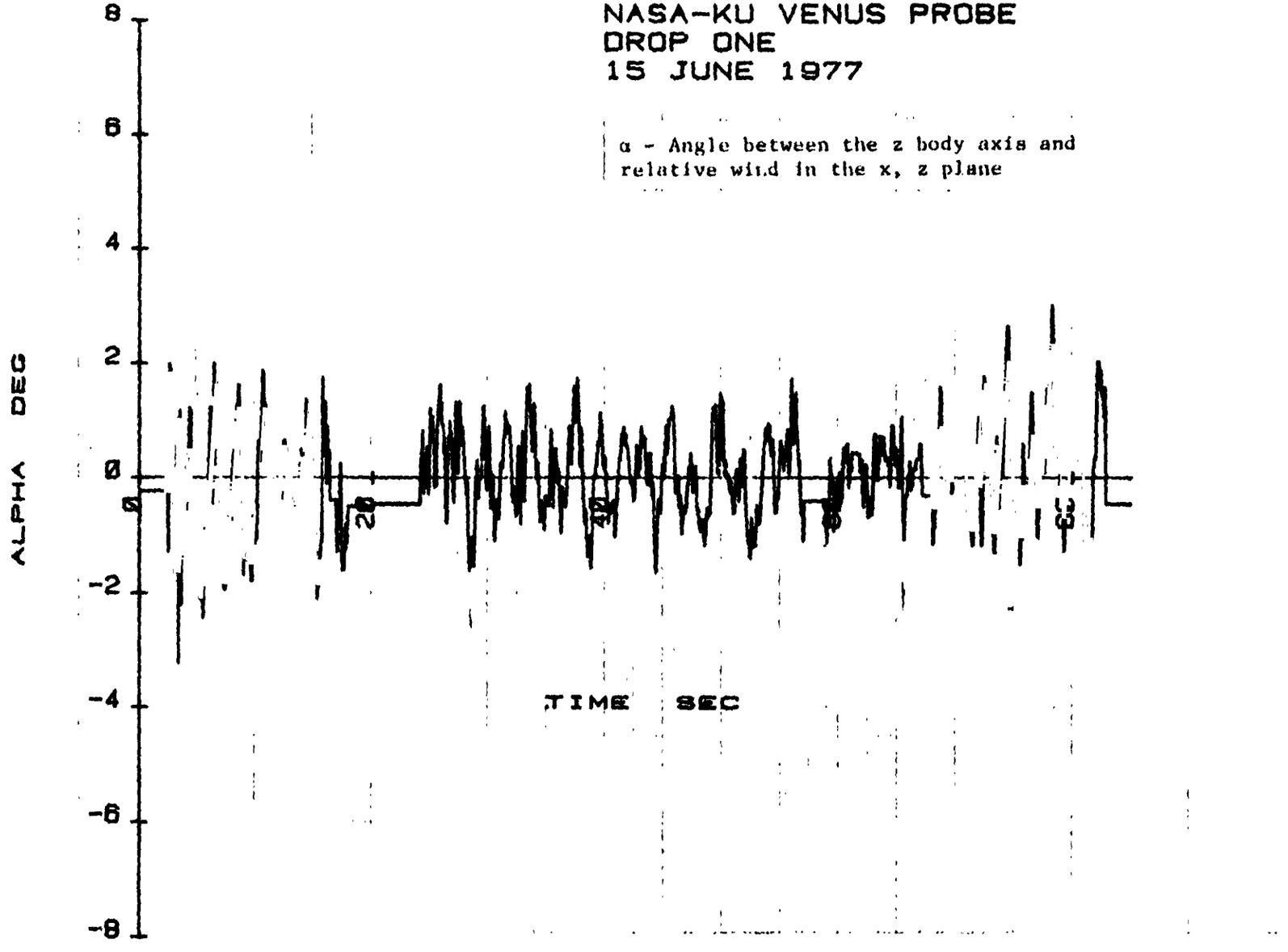

Figure 3.1.8 Small probe angles of attack during flight.

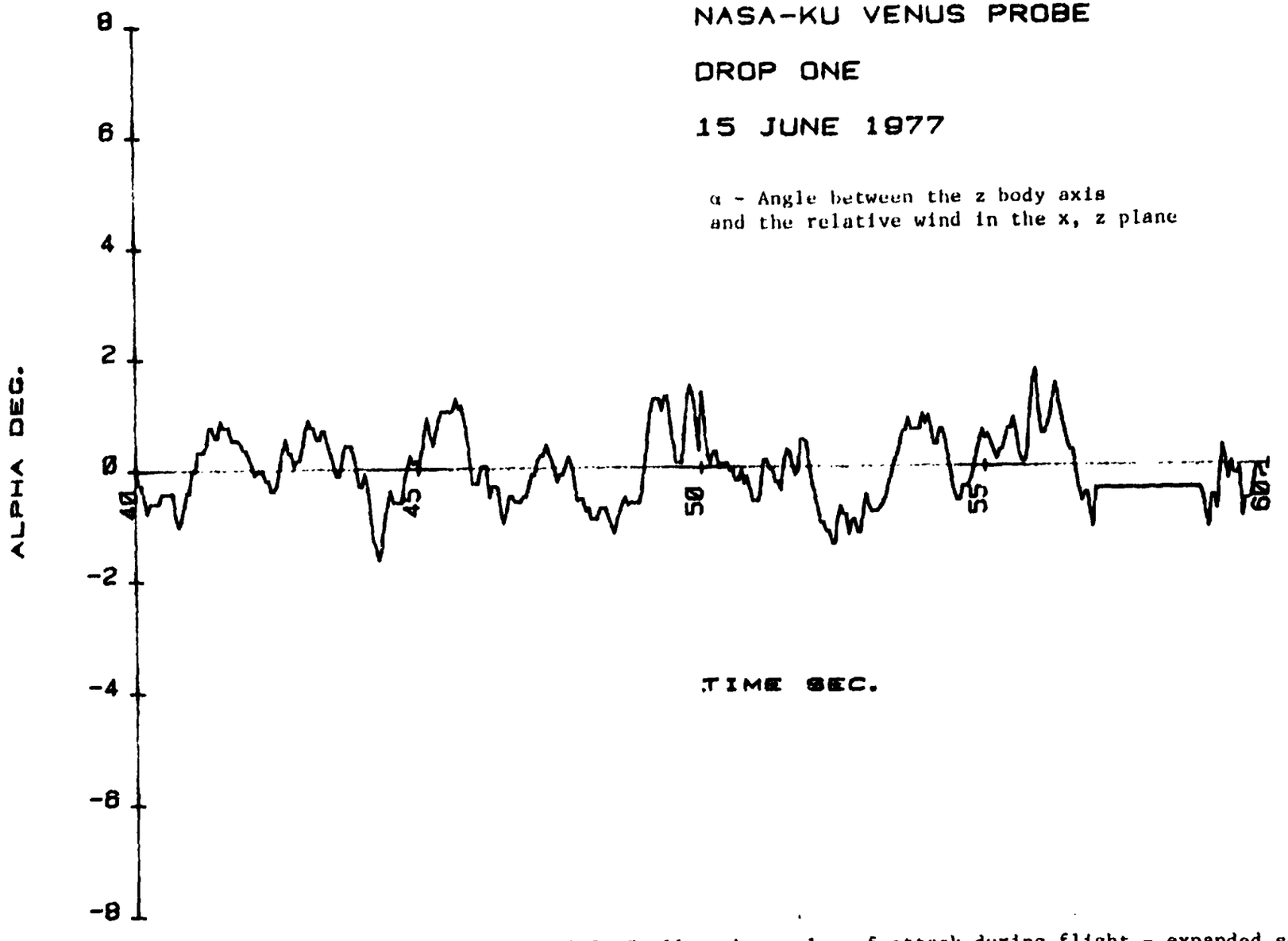

Figure 3.1.9 Small probe angles of attack during flight - expanded scale.

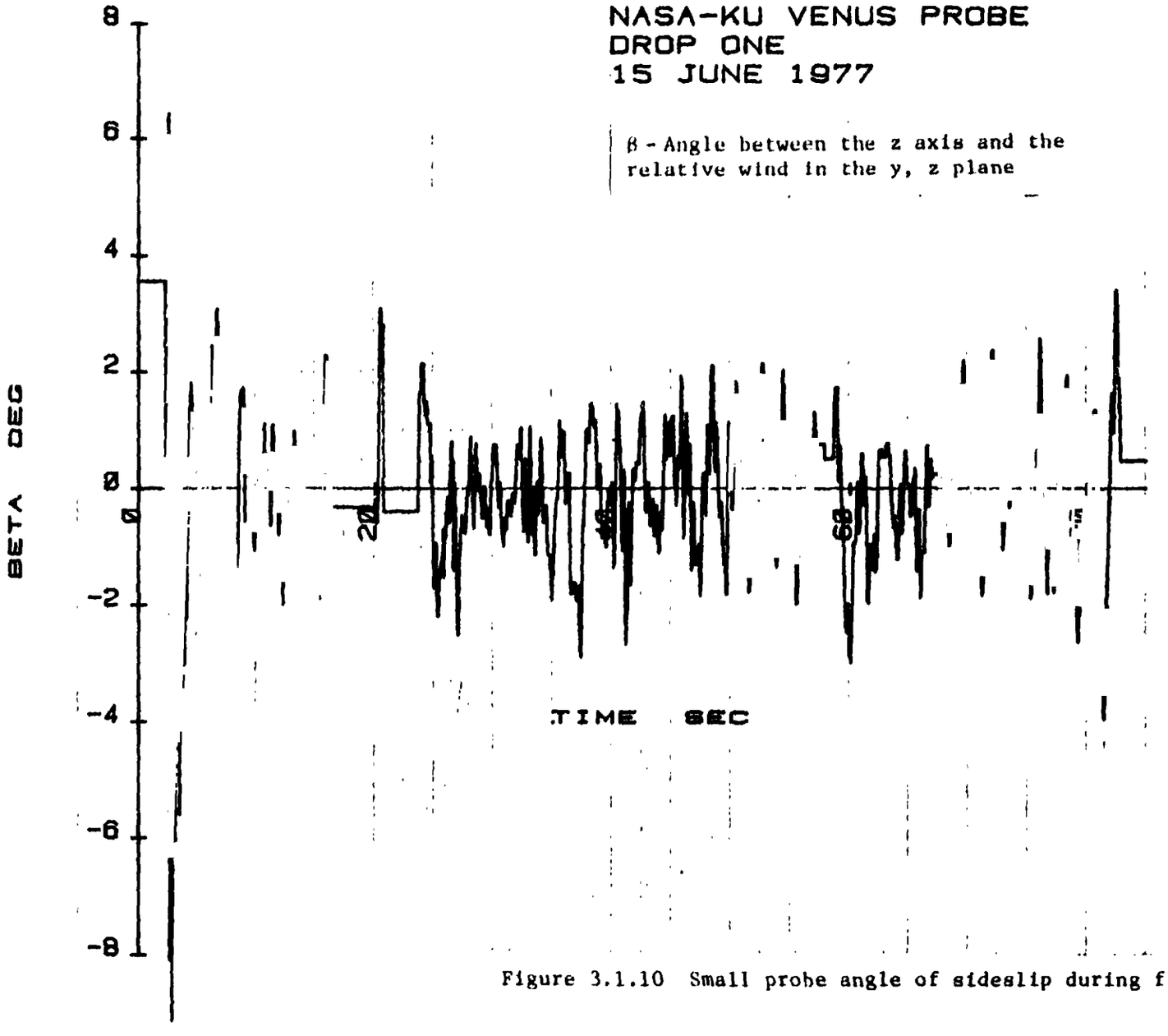

Figure 3.1.10 Small probe angle of sideslip during flight.

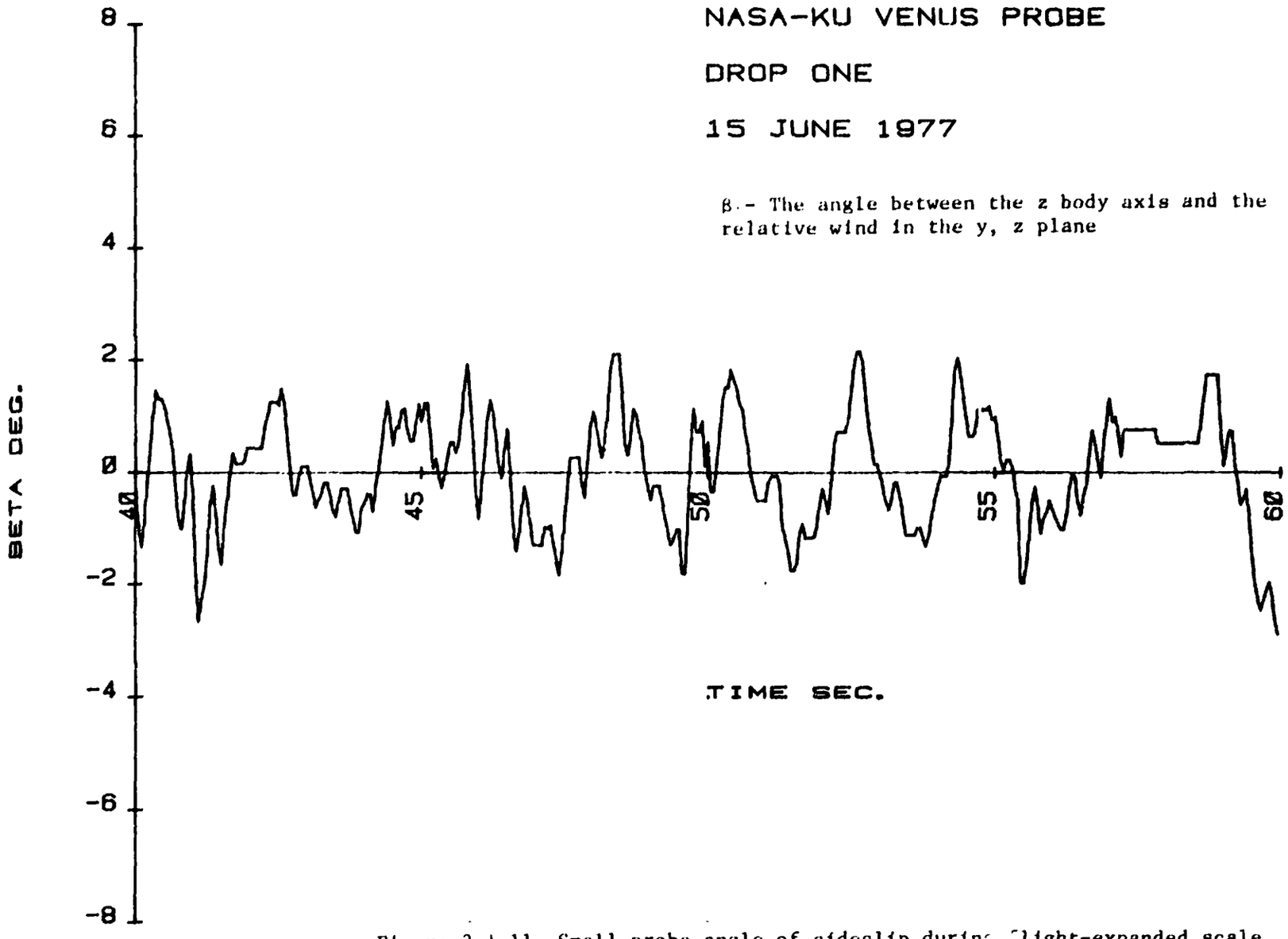

Figure 3.1.11 Small probe angle of sideslip durin[illegible] flight-expanded scale.

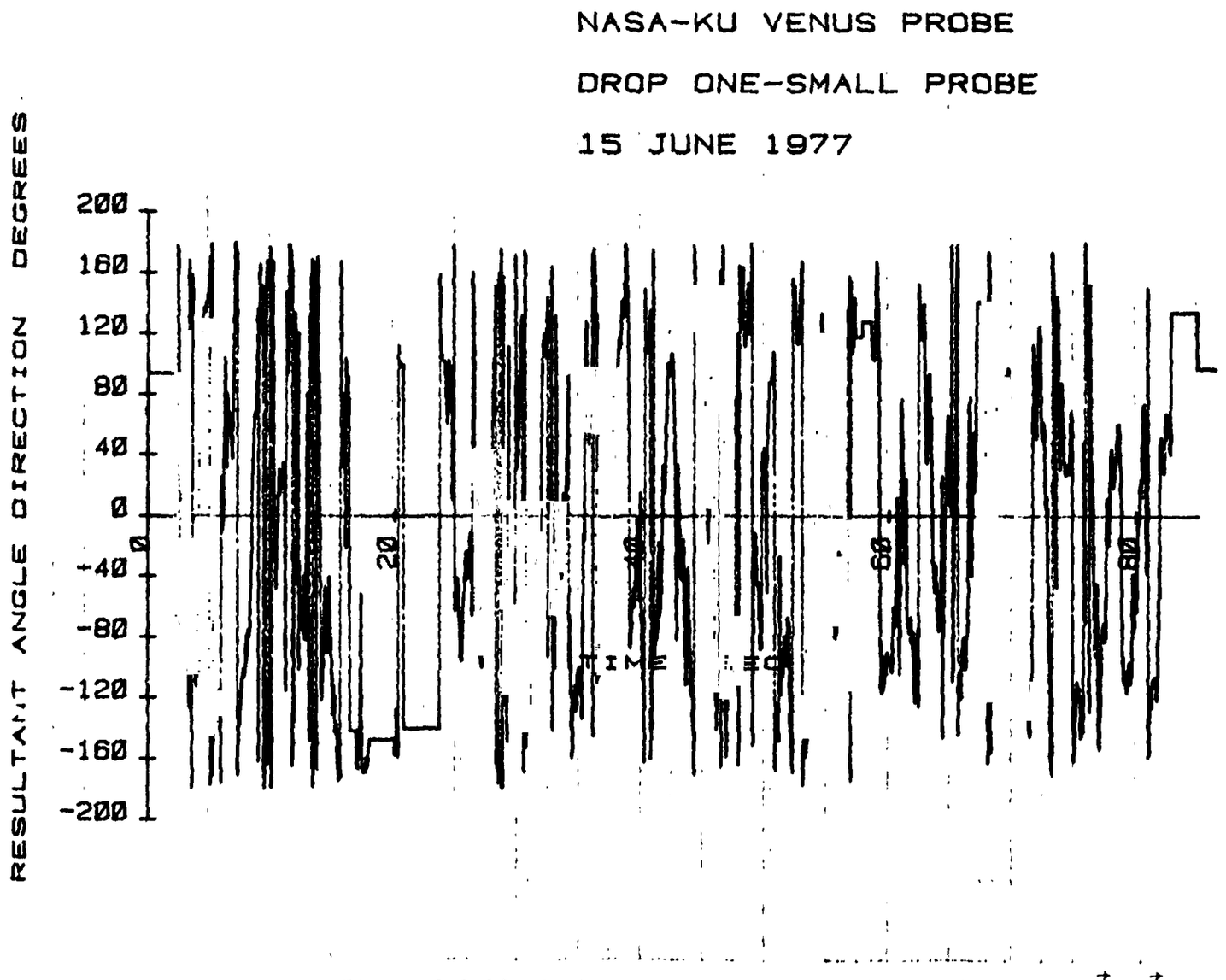

Figure 3.1.12 Small probe resultant angles of direction, $\vec{\alpha} + \vec{\beta}$ (directions from x-axis of resultants of the angles of attack and angles of sideslip).

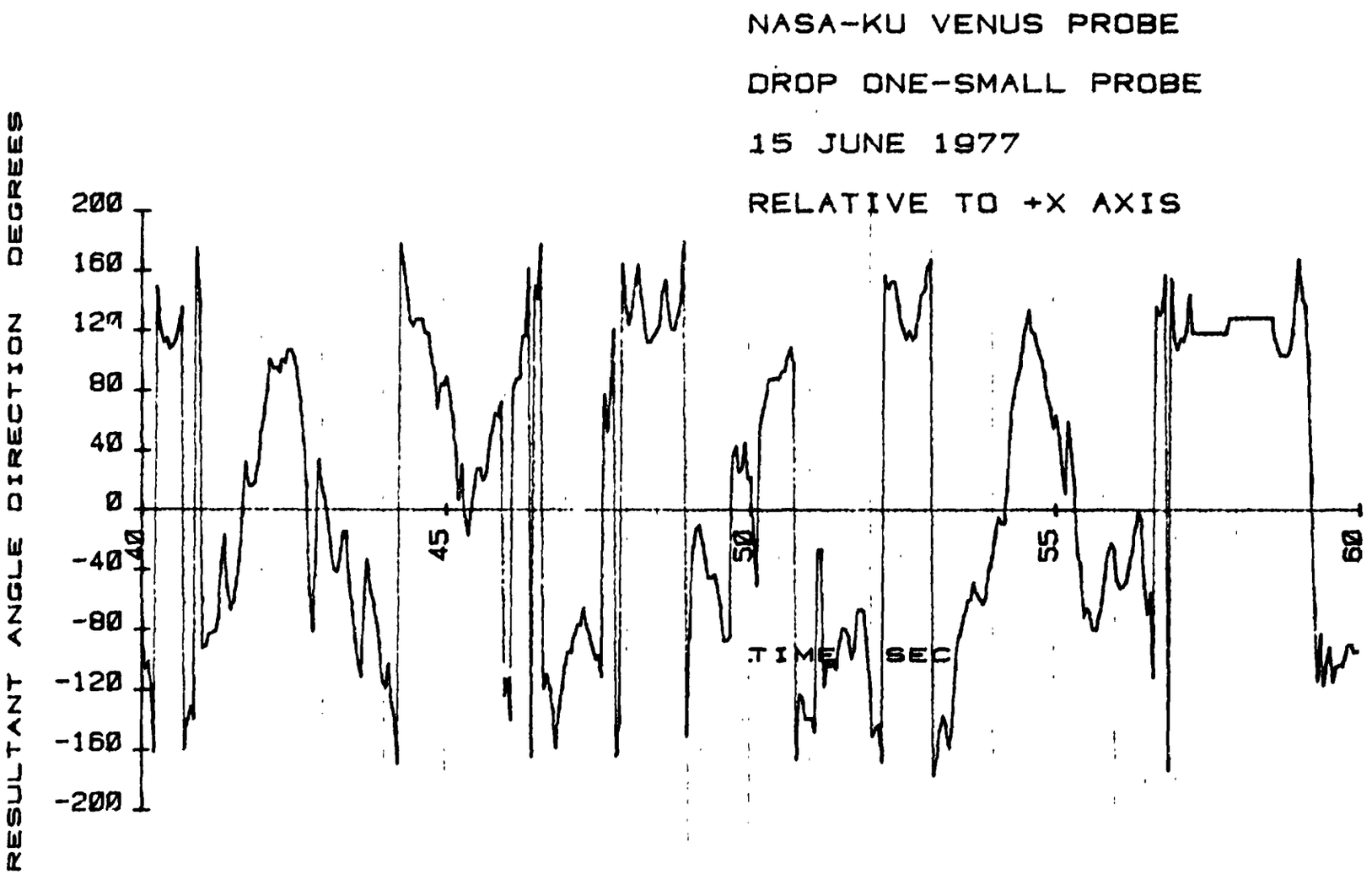

Figure 3.1.13 Small probe resultant angles of direction, $\vec{\alpha} + \vec{\beta}$, (directions from x-axis of resultants of the angles of attack and angles of side-slip) - expanded scale.

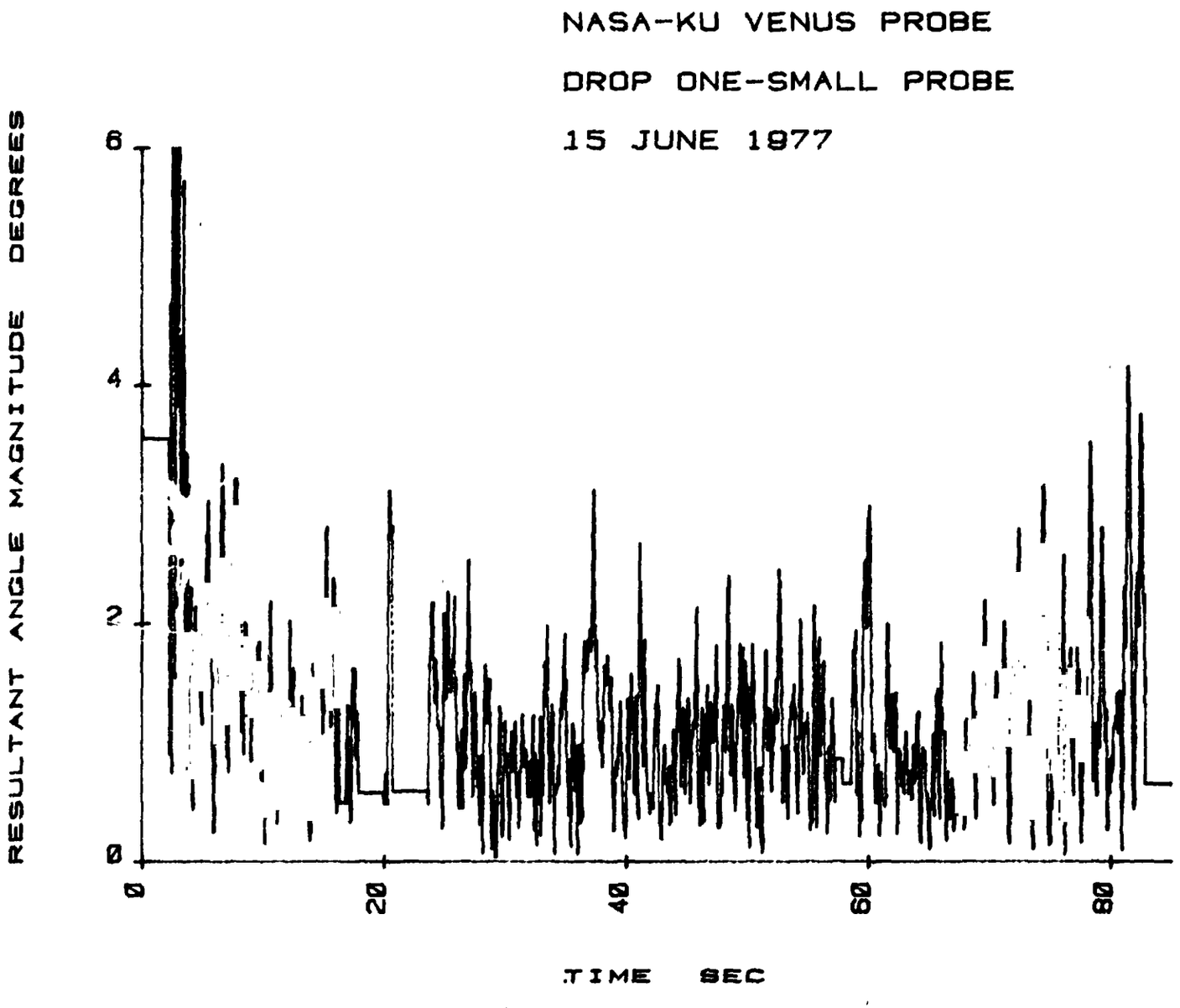

Figure 3.1.14 Small probe resultant angle magnitudes, $|\vec{\alpha} + \vec{\beta}|$.

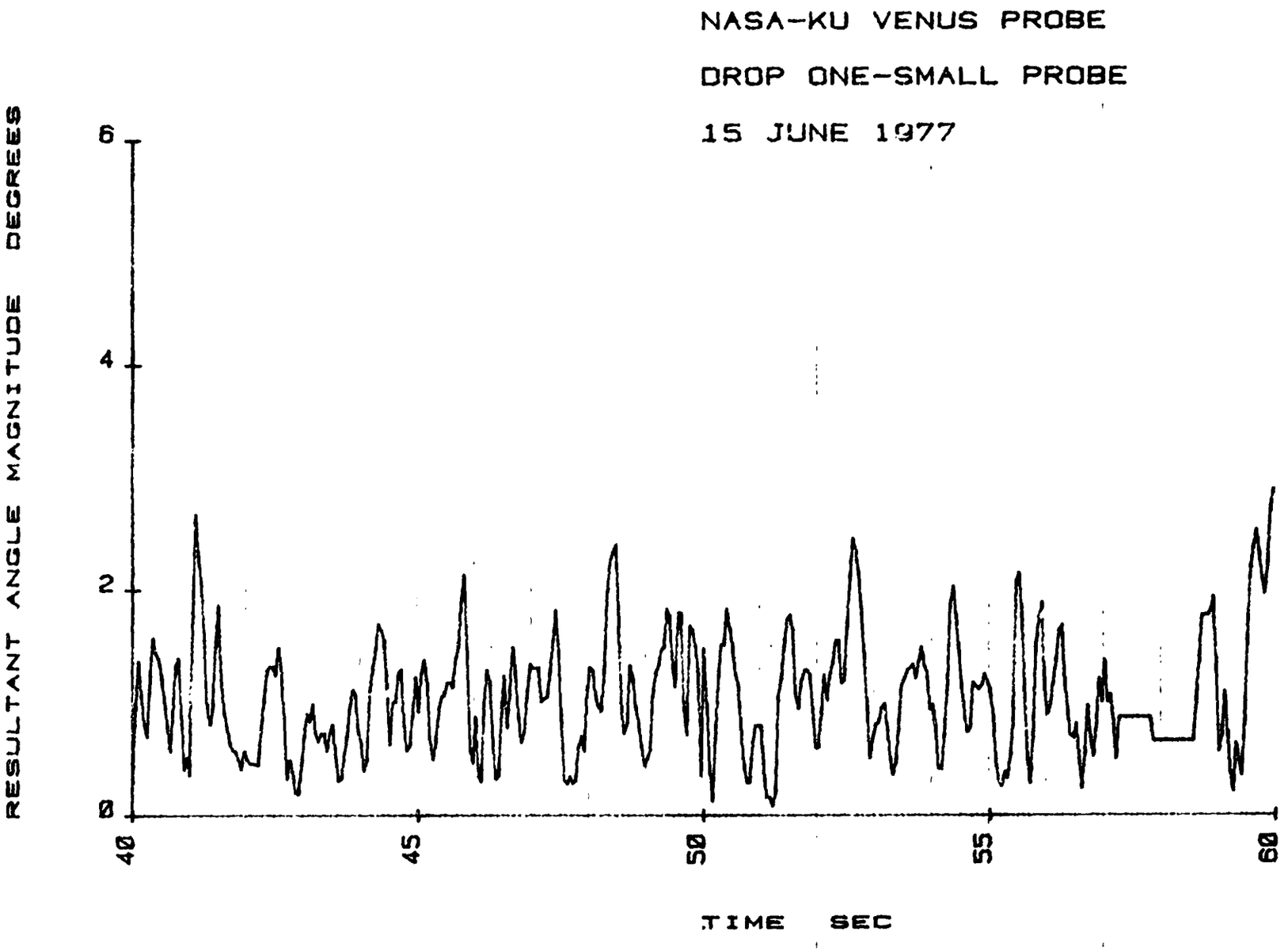

Figure 3.1.15 Small probe resultant angle magnitudes, $|\vec{\alpha} + \vec{\beta}|$, expanded scale.

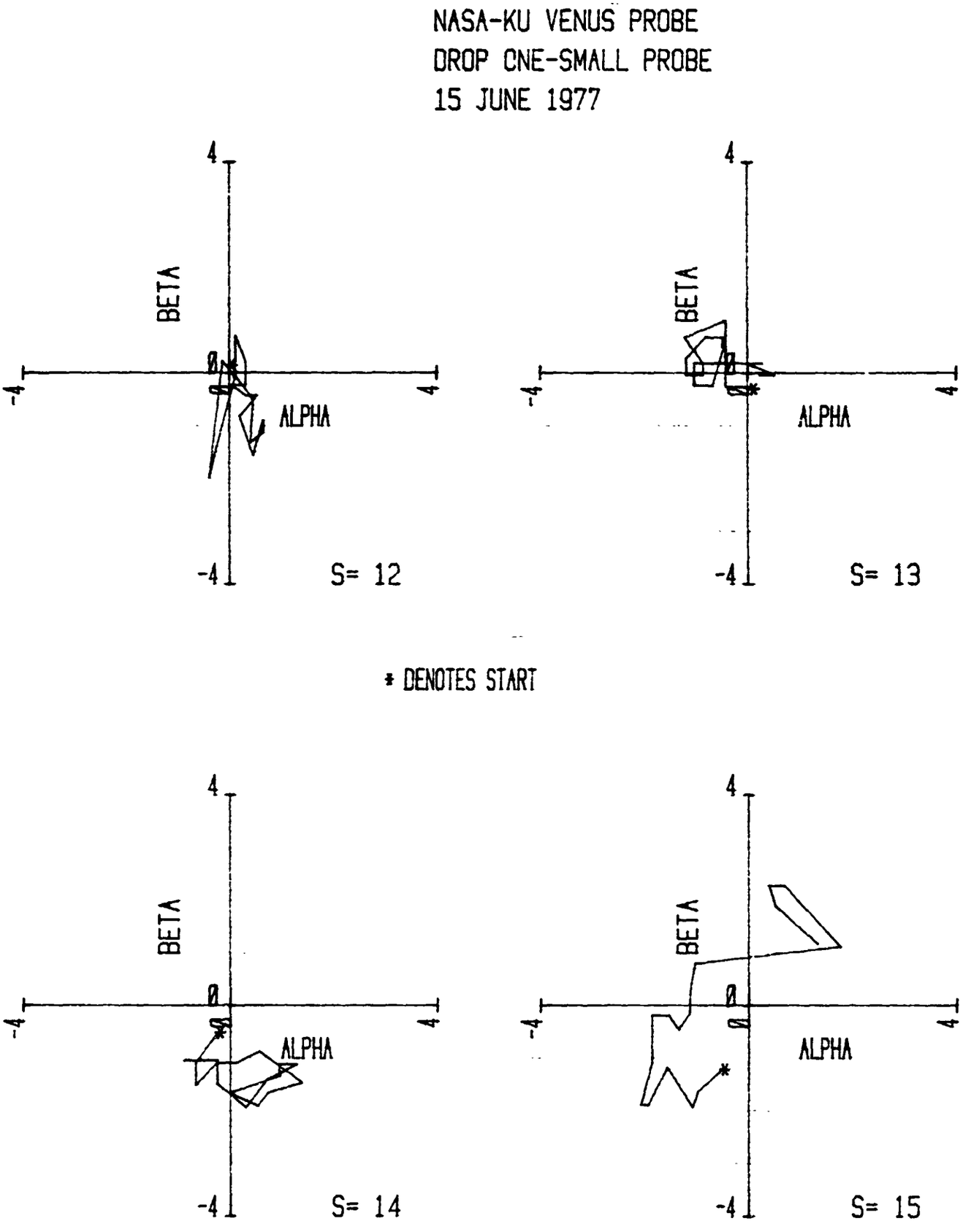

Figure 3.1.16 Small probe resultant vector, $\vec{\alpha} + \vec{\beta}$, motion, 12 through 15 seconds.

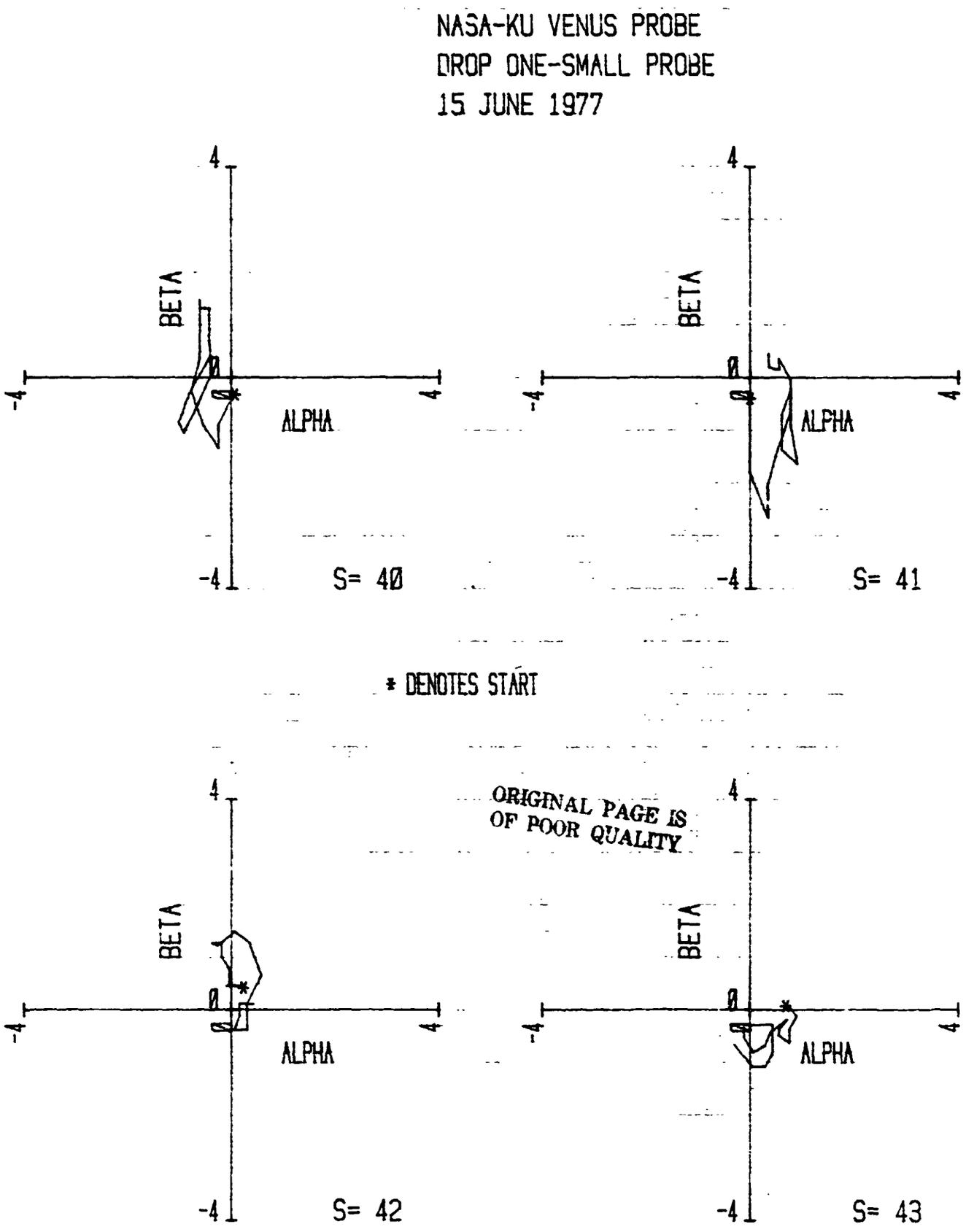

Figure 3.1.17 Small probe resultant vector, $\vec{\alpha} + \vec{\beta}$, motion, 40 through 43 seconds.

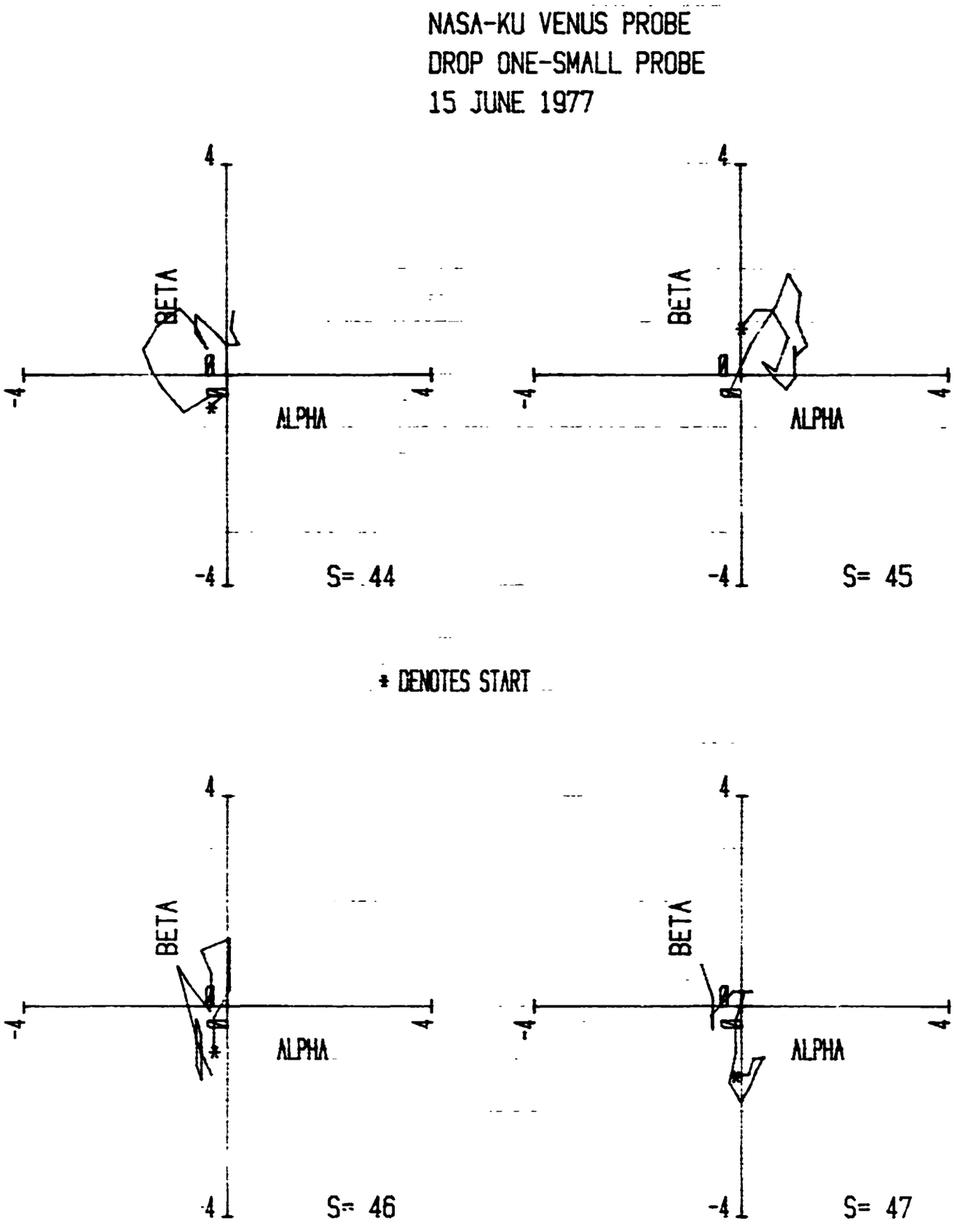

Figure 3.1.18 Small probe resultant vector, $\vec{\alpha} + \vec{\beta}$, motion, 44 through 47 seconds.

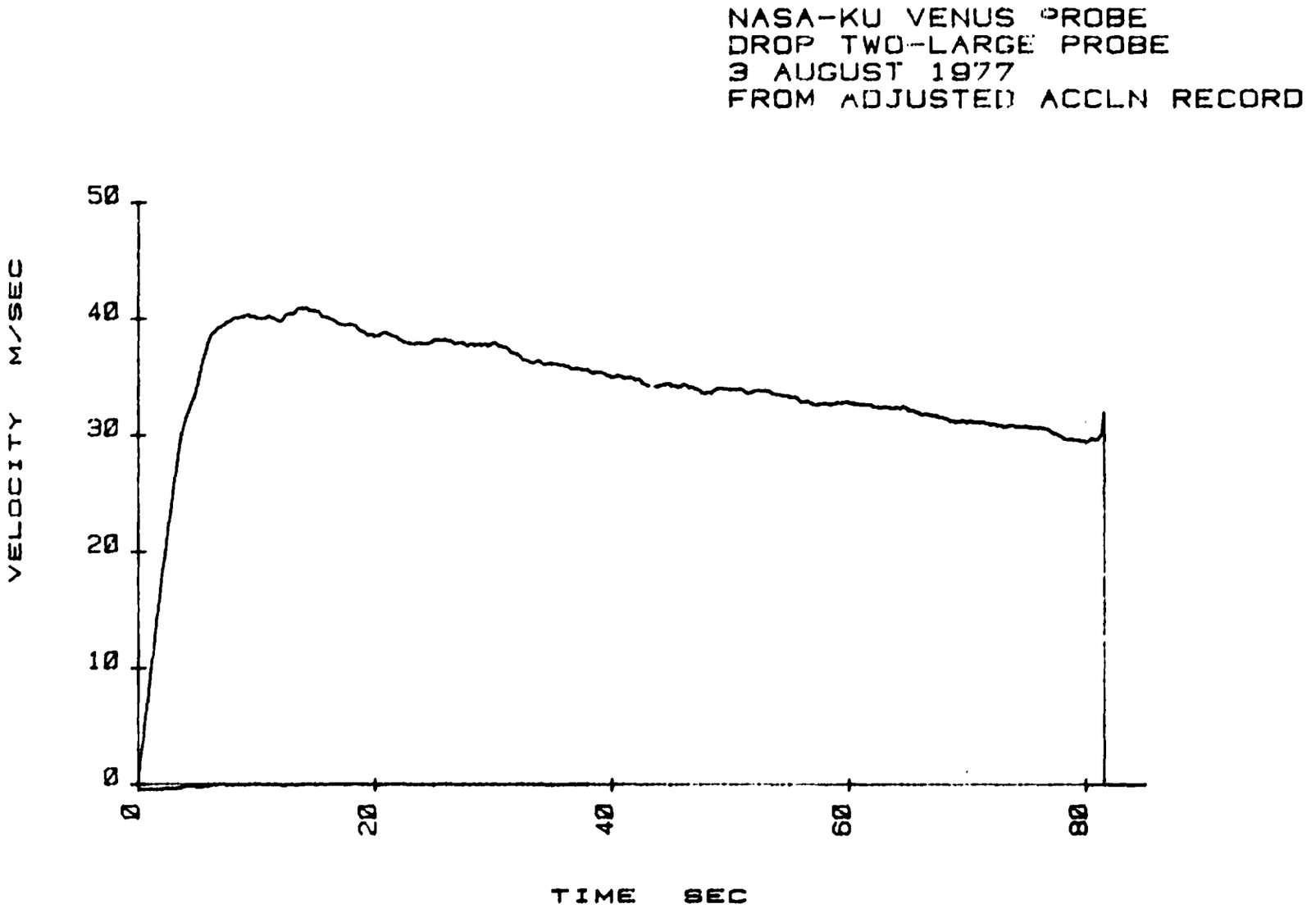

Figure 3.2.1 Large probe velocity from accelerometer data.

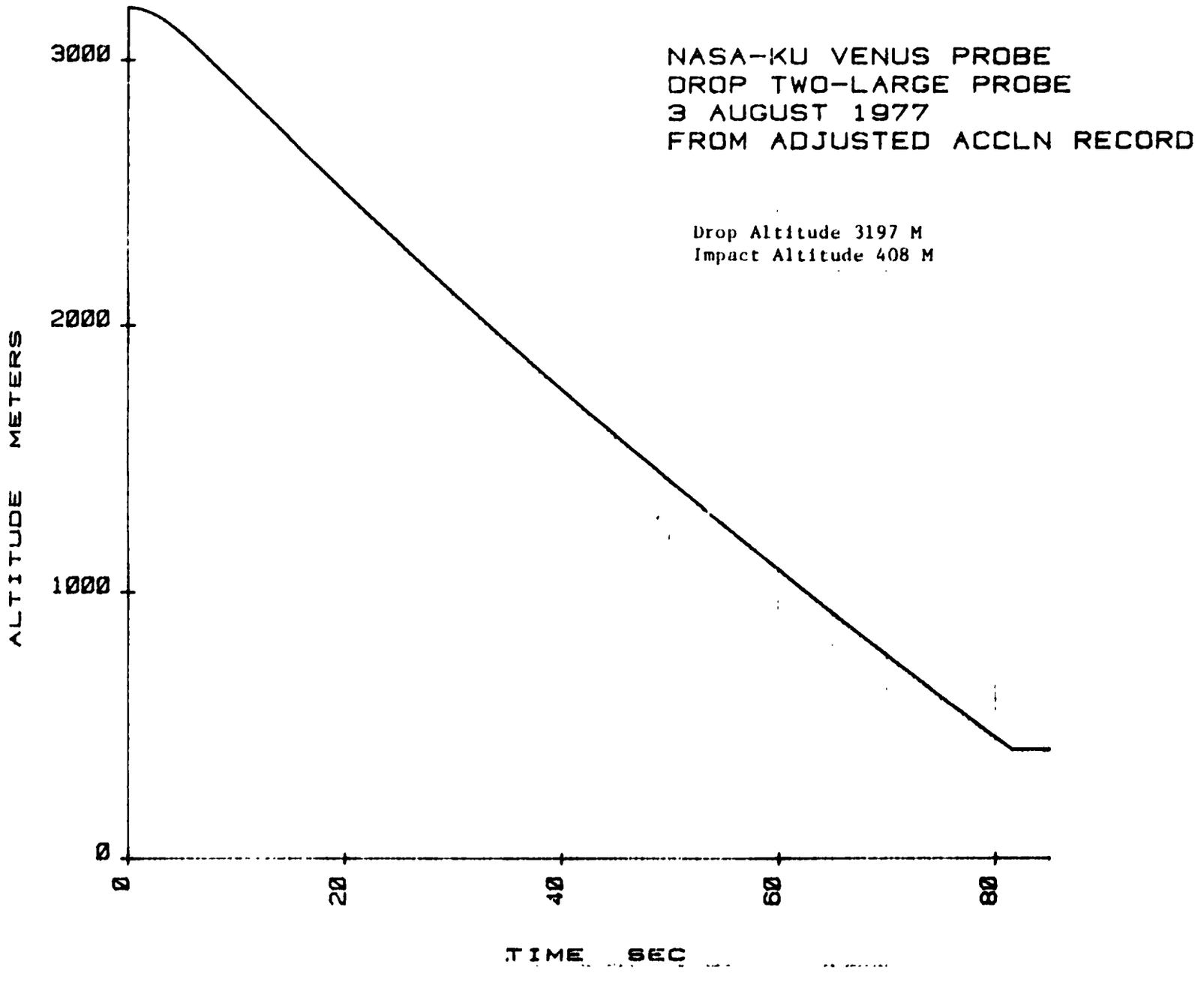

Figure 3.2.2 Large probe altitude from accelerometer data.

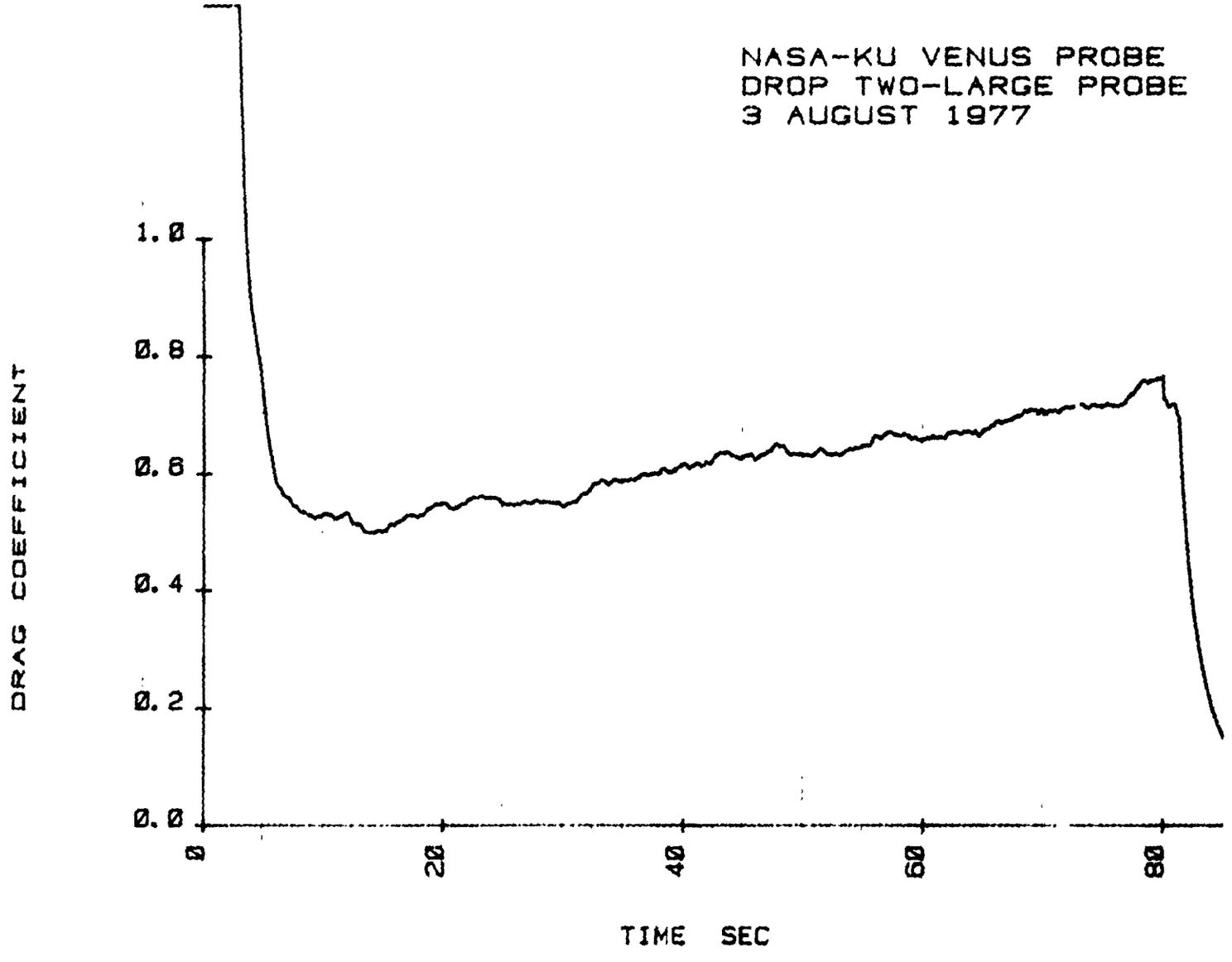

Figure 3.2.3 Large probe drag coefficient from accelerometer data.

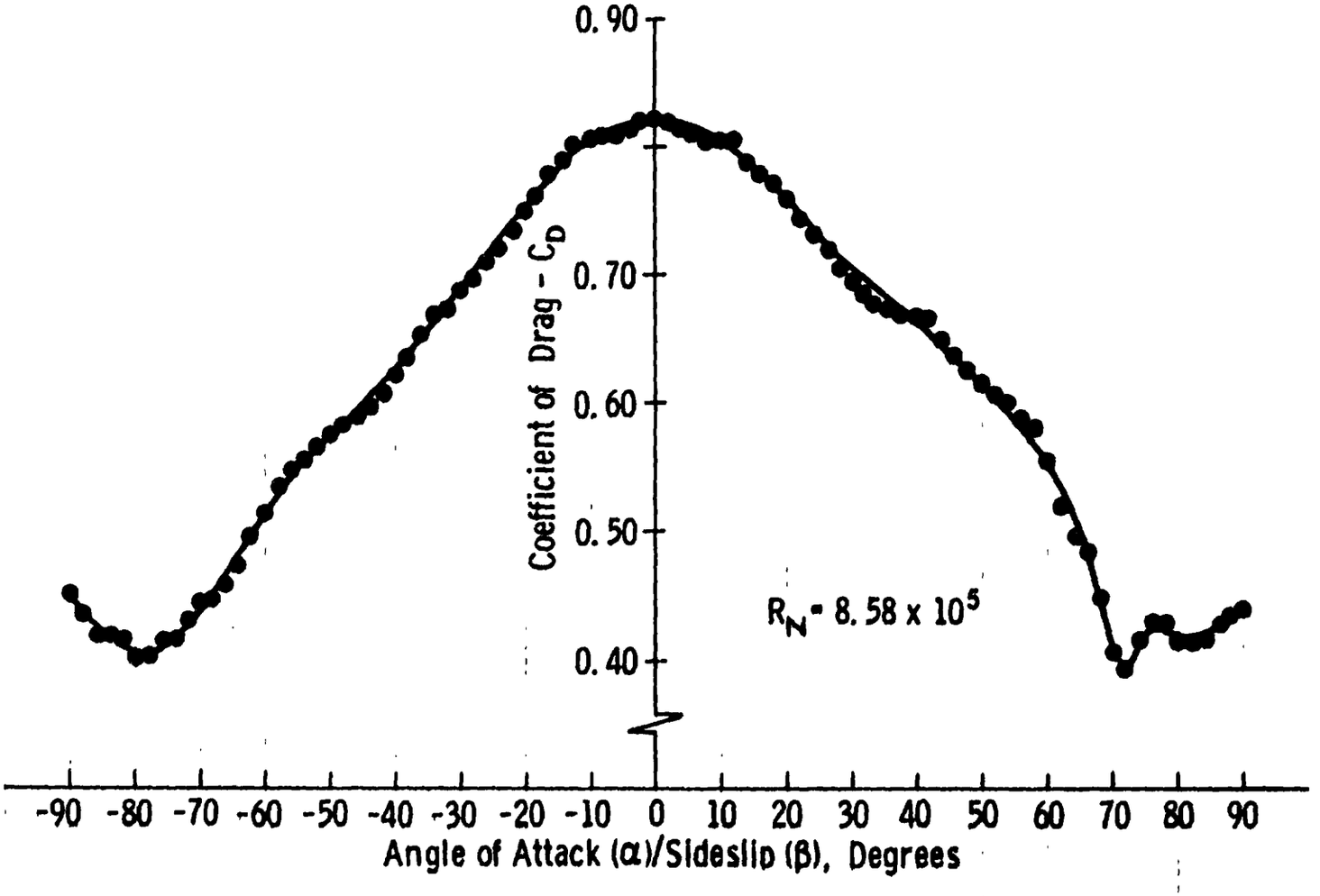

Figure 3.2.4. Large Probe Drag Coefficient from Wind Tunnel Data.

Figure 3.2.5 Large probe lift coefficient (resultant of lift and side force.

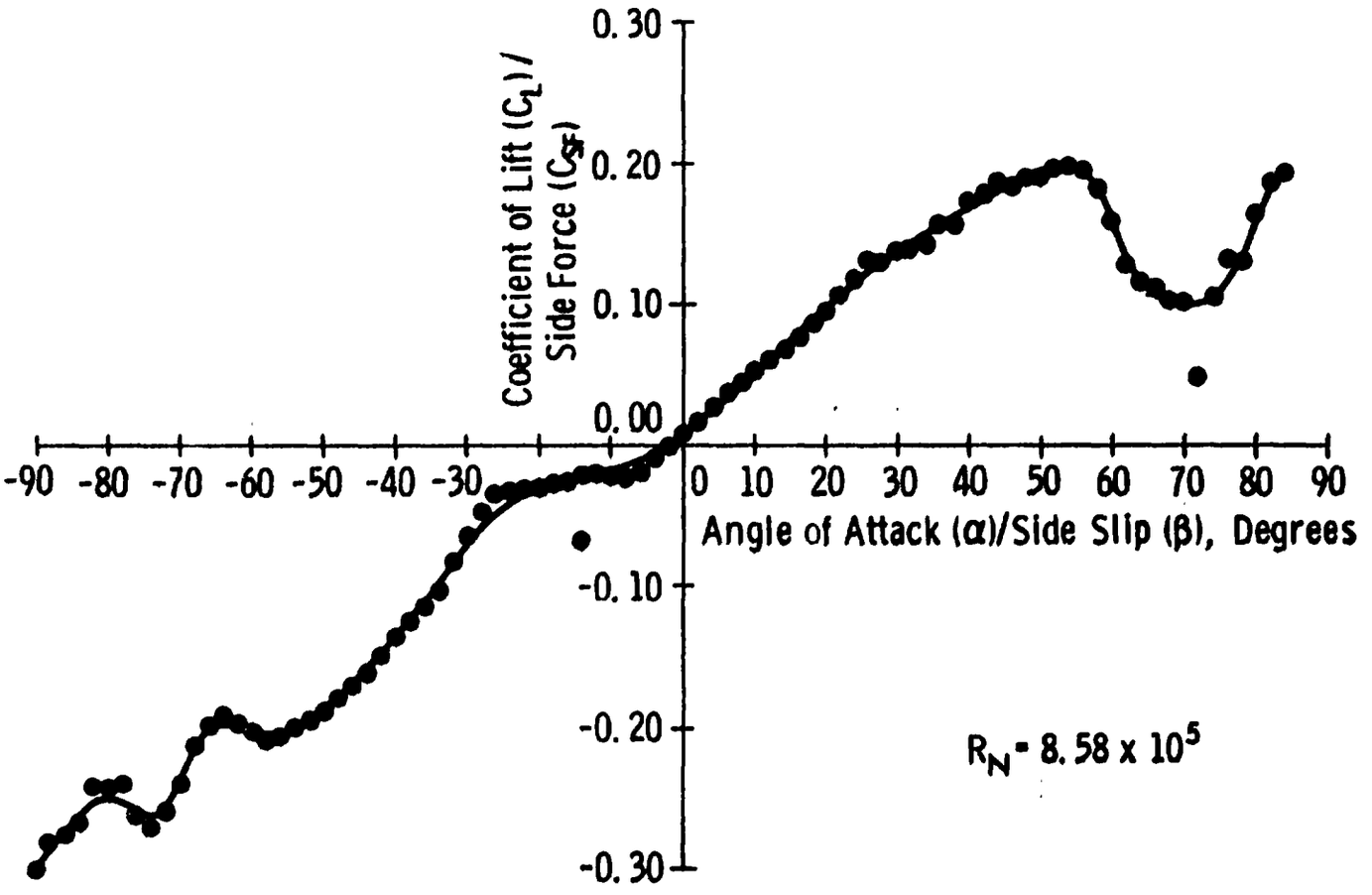

Figure 3.2.6. Large Probe Lift Coefficient from Wind Tunnel Data.

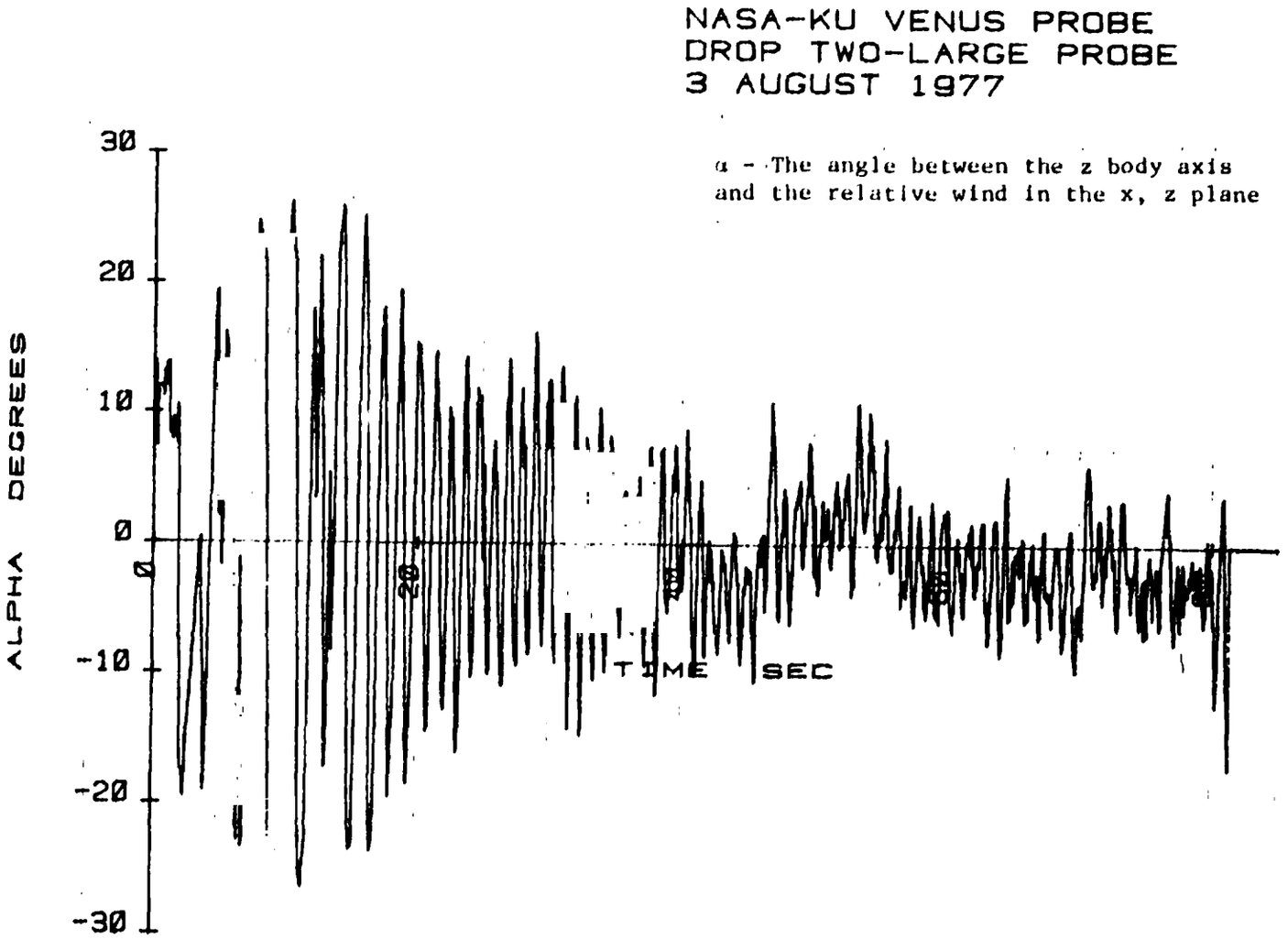

Figure 3.2.7 Large probe angles of attack during flight.

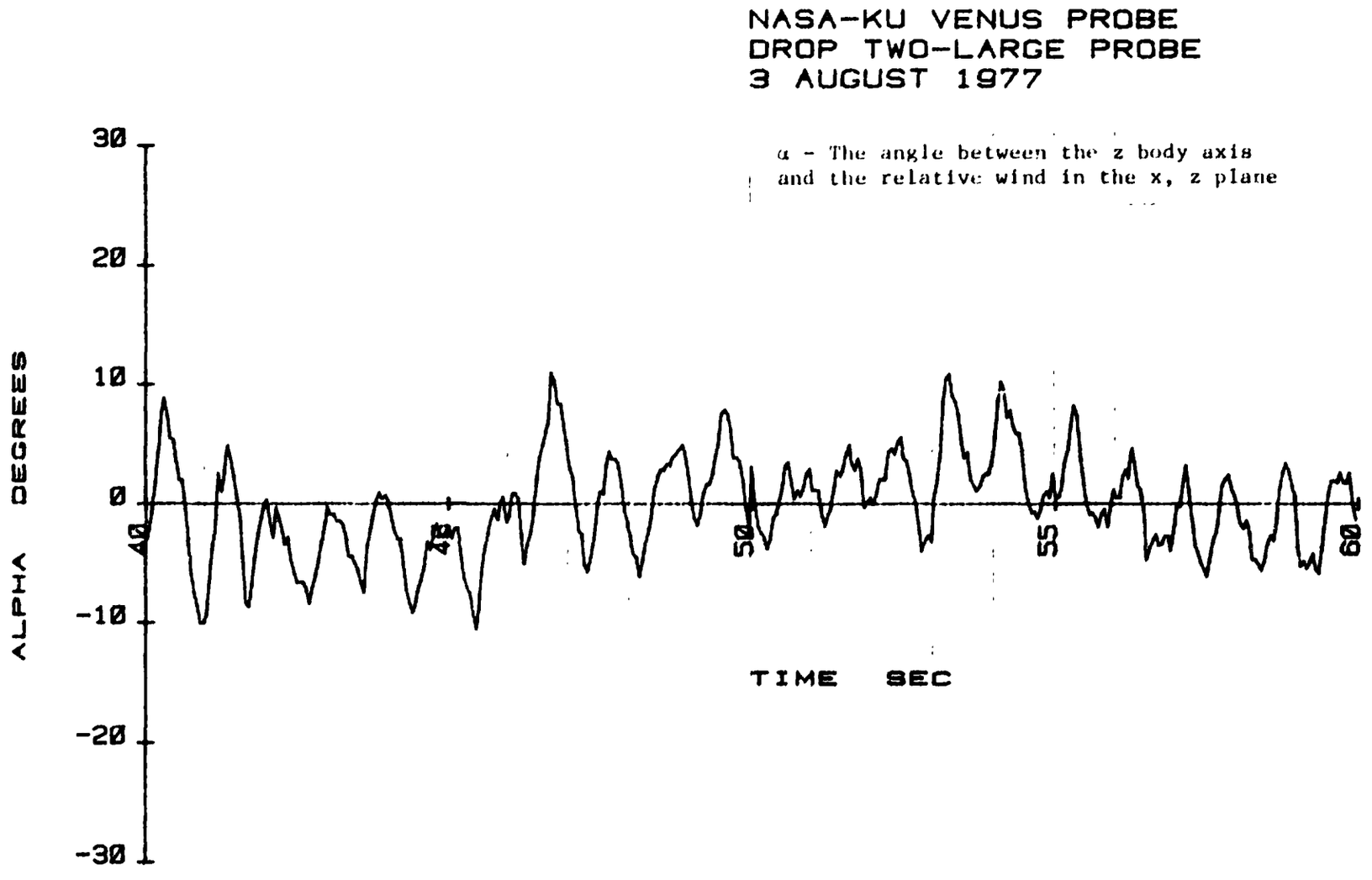

Figure 3.2.8 Large probe angles of attack during flight - expanded scale.

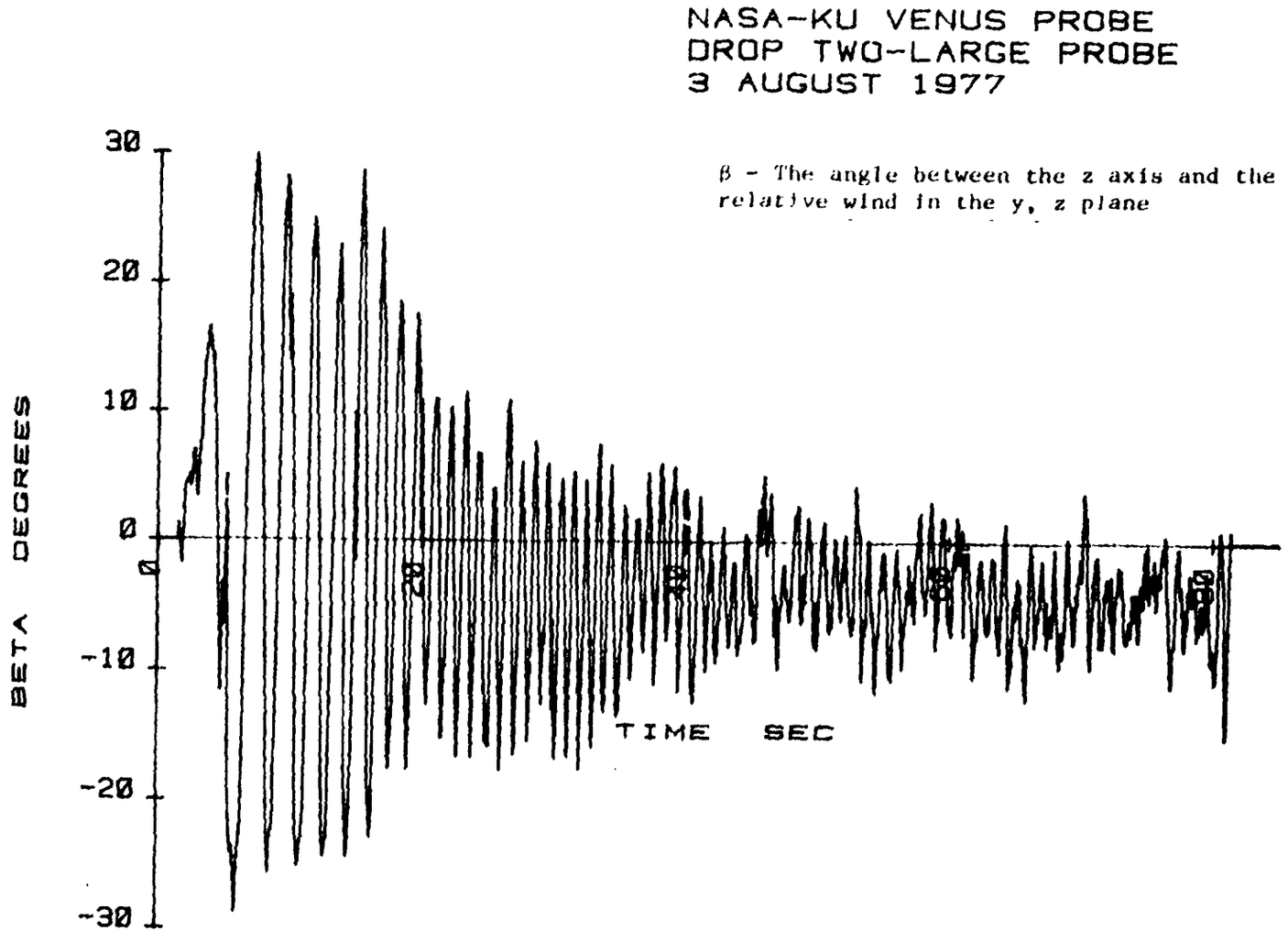

Figure 3.2.9 Large probe angles of sideslip during flight.

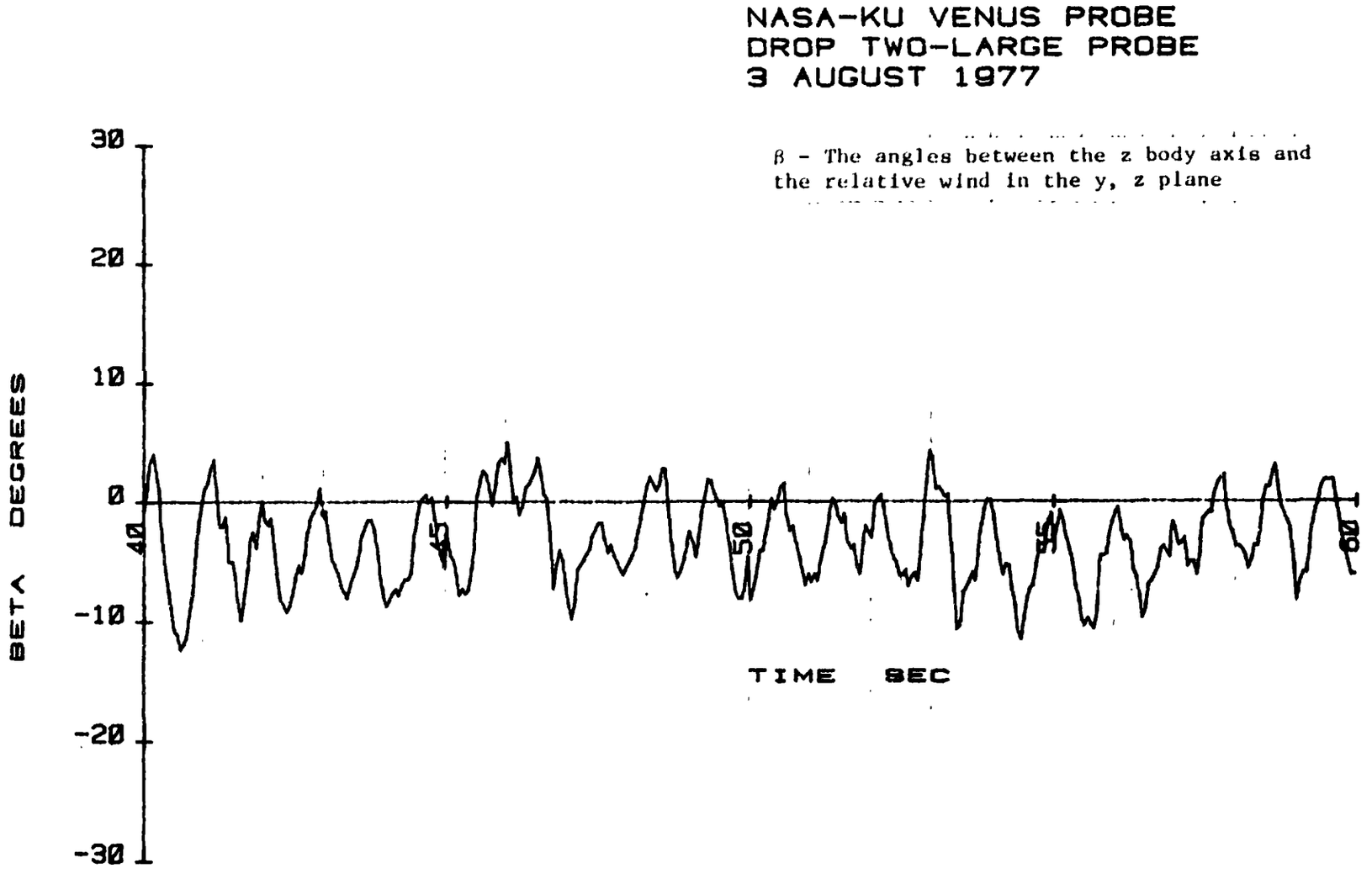

Figure 3.2.10 Large probe angles of sideslip during flight - expanded scale.

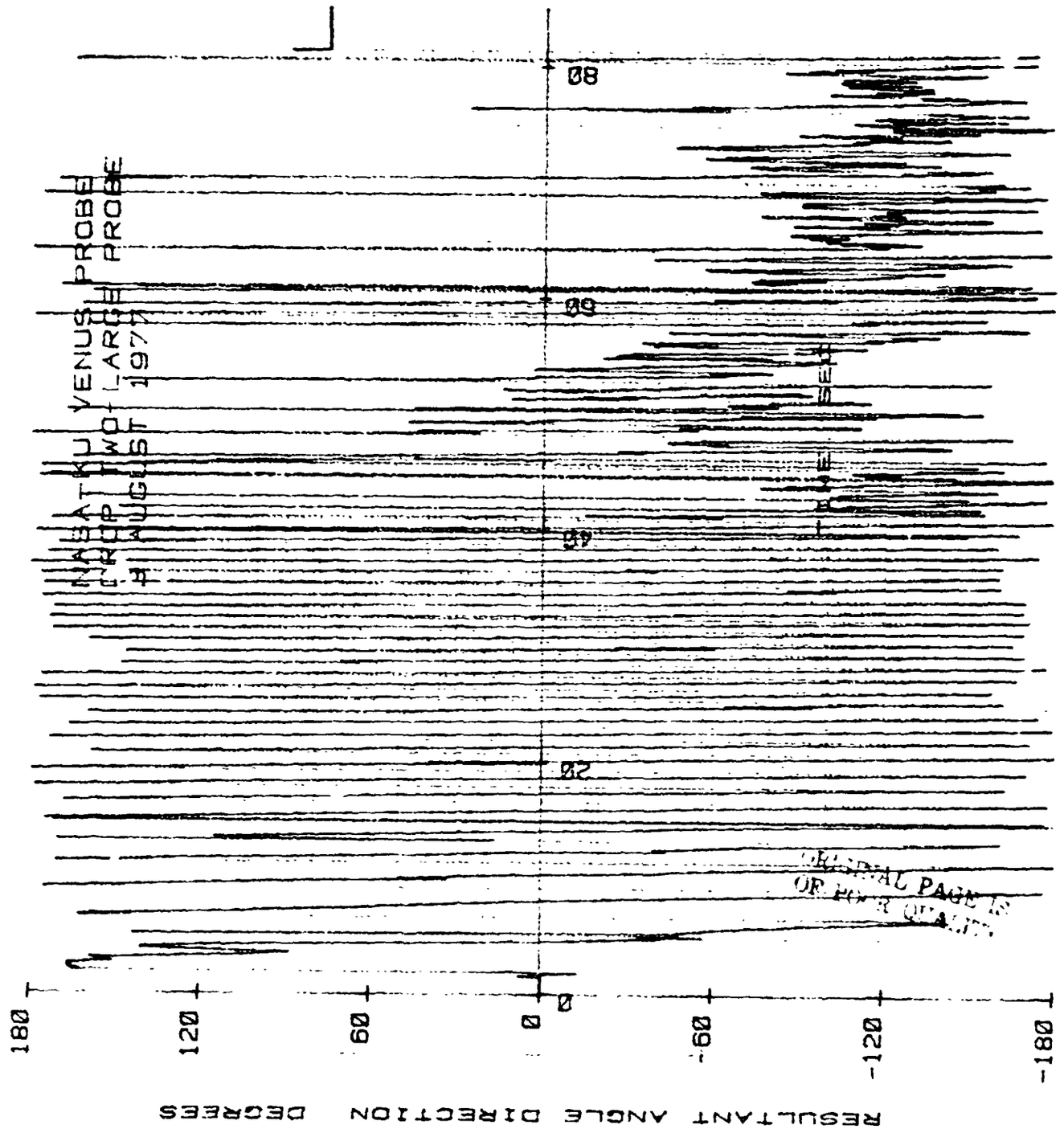

Figure 3.2.11 Large probe resultant angles of direction, $\vec{\alpha} + \vec{\beta}$, (directions from the x axis of resultants of angles of attack and angles of sideslip).

Figure 3.2.12 Large probe resultant angles of direction, $\vec{\alpha} + \vec{\beta}$, (directions from the x axis of resultants of angles of attack and angles of sideslip) expanded scale.

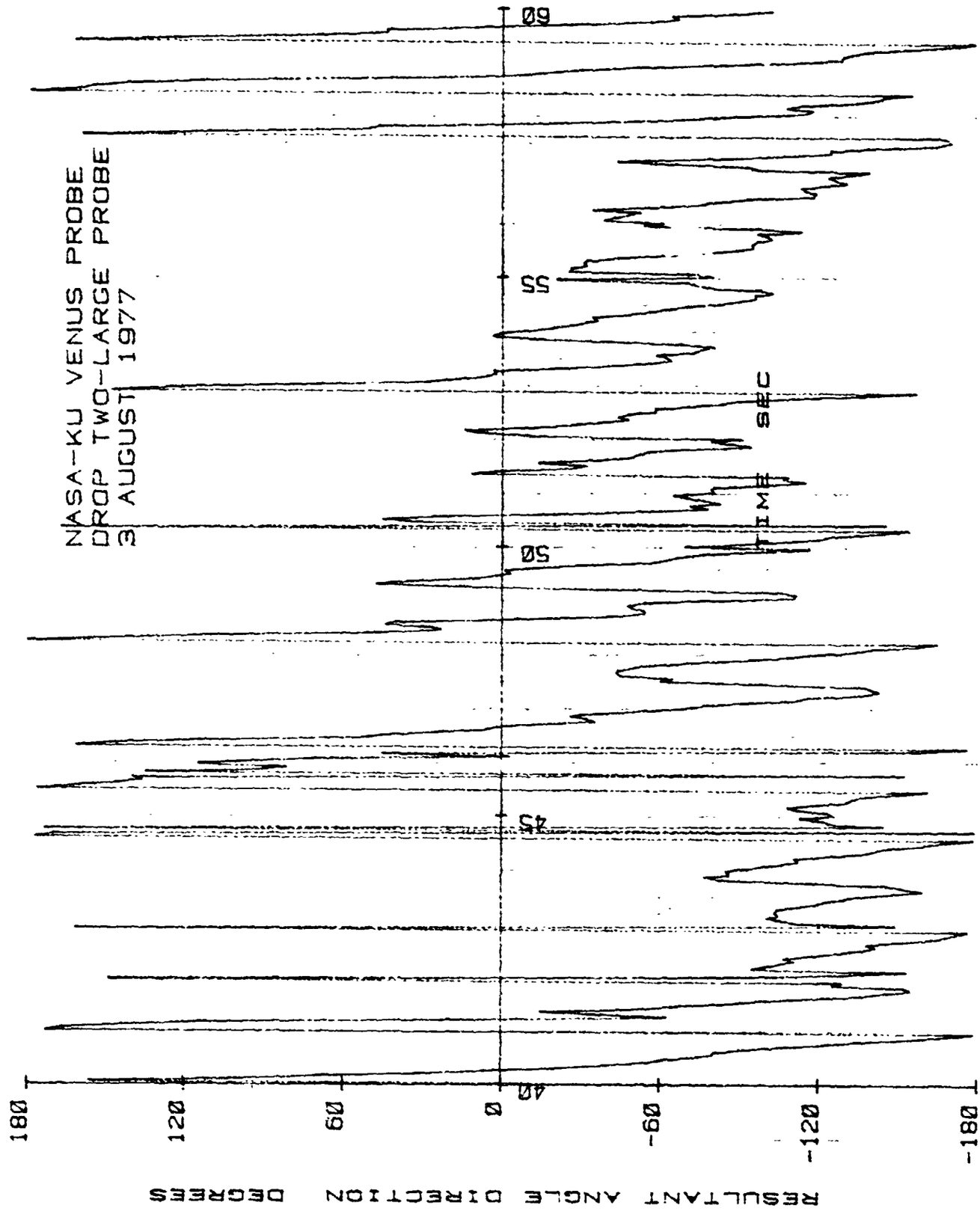

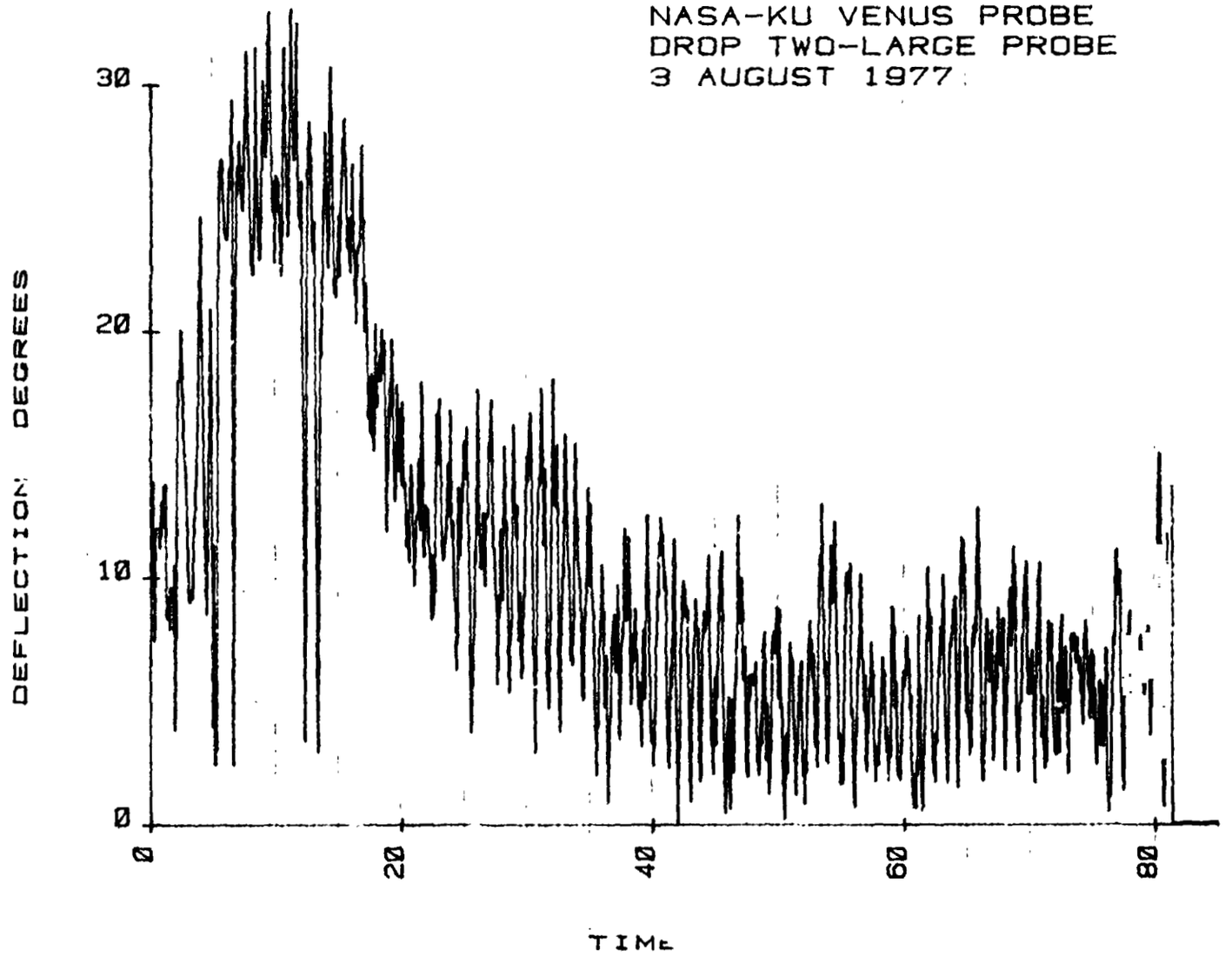

Figure 3.2.13 Large probe resultant angle magnitude, $|\vec{\alpha} + \vec{\beta}|$.

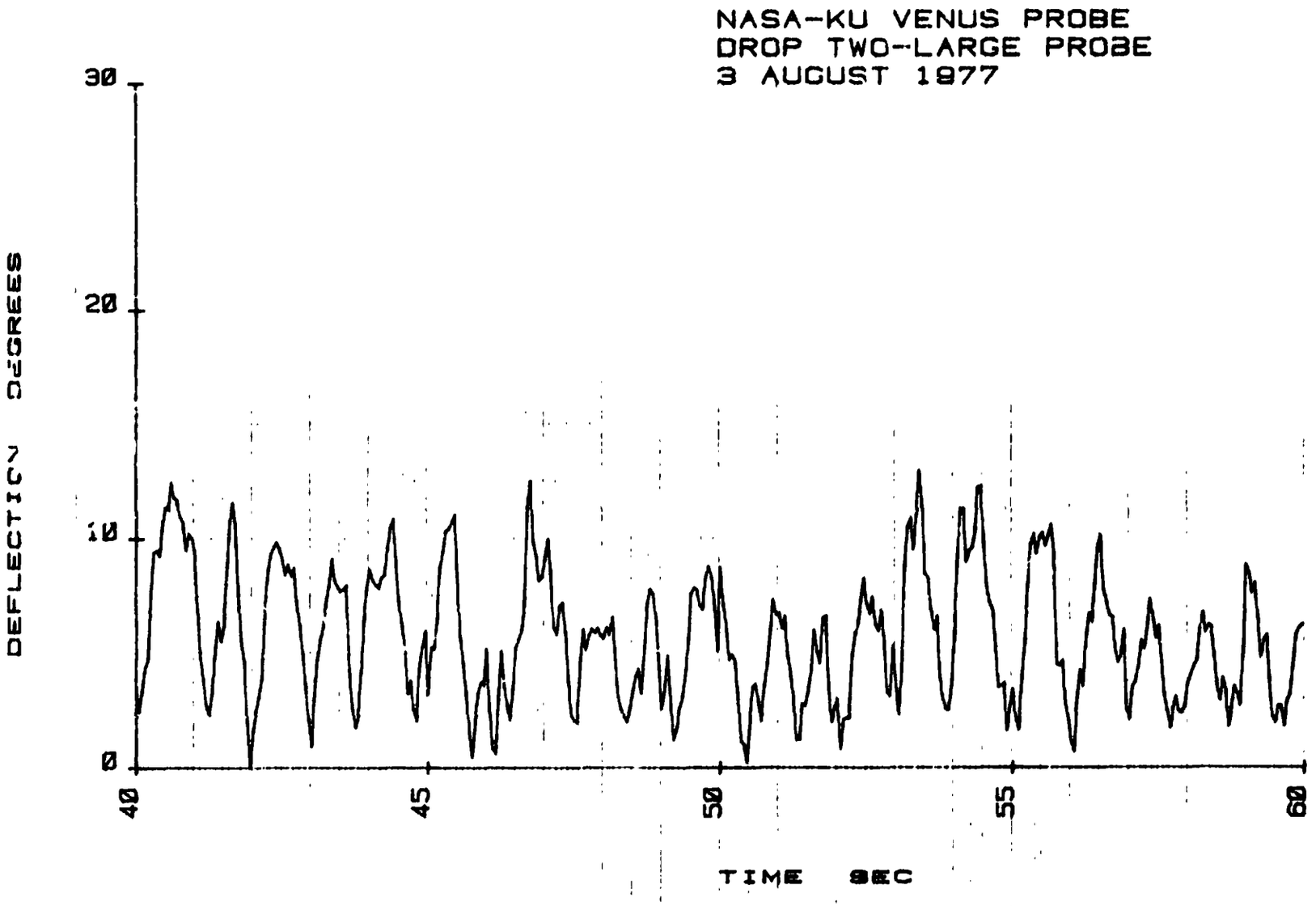

Figure 3.2.14 Large probe resultant angle magnitude, $|\vec{\alpha} + \vec{\beta}|$ expanded scale.

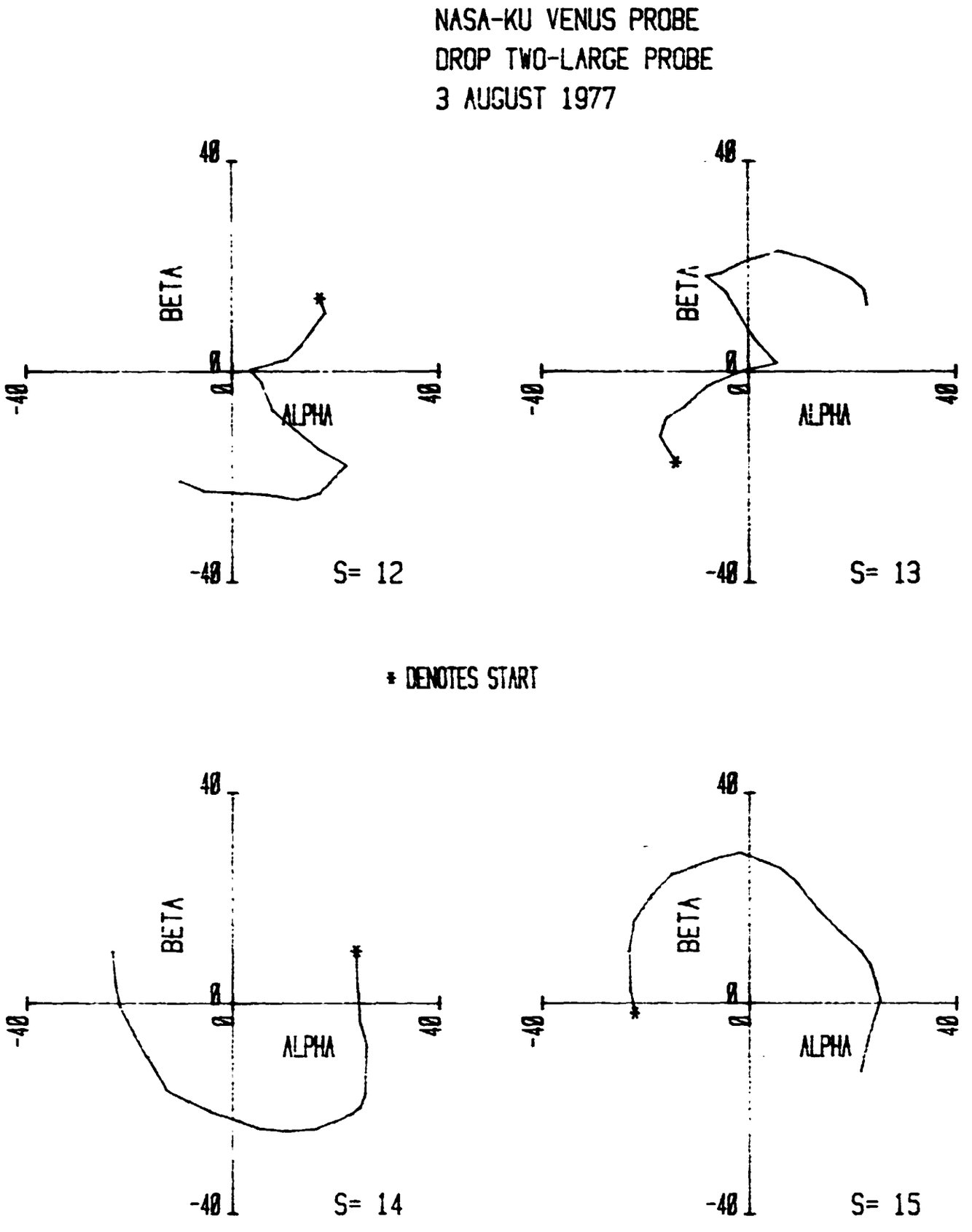

Figure 3.2.15 Large probe resultant vector, $\vec{x} + \vec{s}$, motion, 12 through 15 seconds.

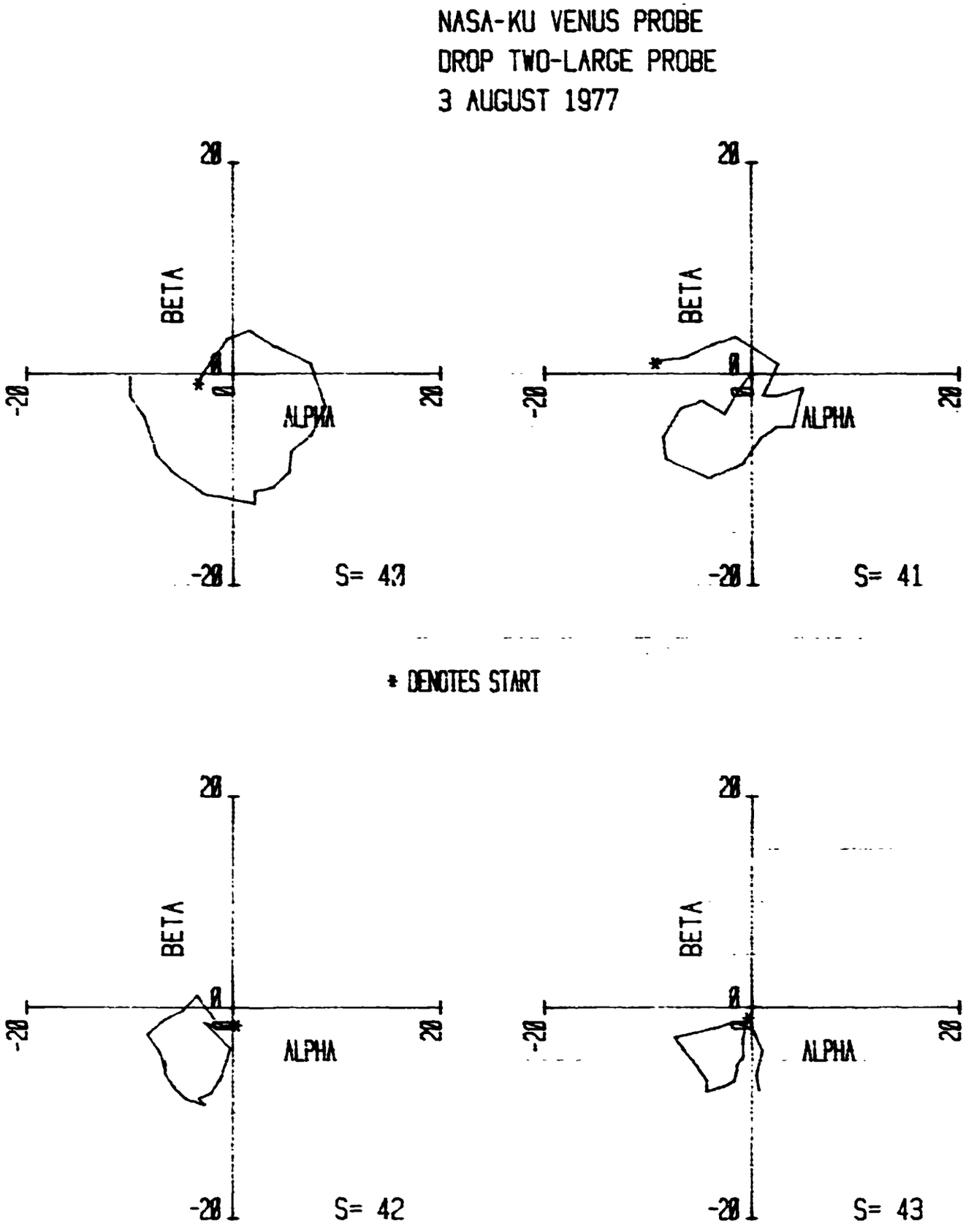

Figure 3.2.16 Large probe resultant vector, $\vec{\alpha} + \vec{\beta}$, motion, 40 through 43 seconds.

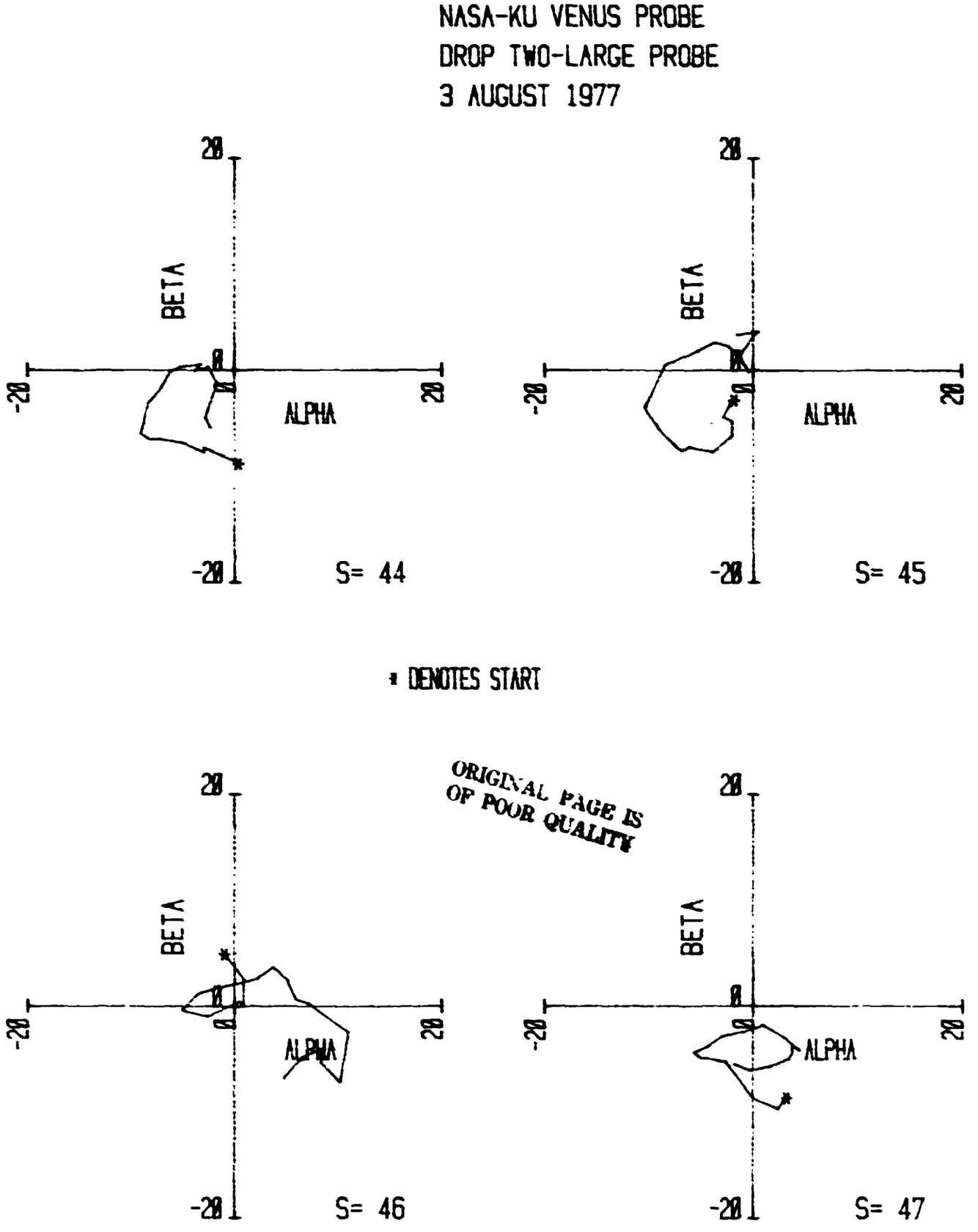

Figure 3.2.17 Large probe resultant vector, $\vec{\omega}$ motion, 44 through 47 seconds.

Table I Probe Model Data

Item	Small Probe	Large Probe
Drop date	15 June, 1977	3 August, 1977
Diameter	1.50m (59.06")	1.49m (58.5")
Area	1.76^2m (19 sq. ft.)	$1.73m^2$ (18.66 sq.ft.)
Weight	74.1 kg (163 lb)	67.0 kg (147.4 lb)
C.G. (ahead of separation)	.058m (2.3")	.157m (6.2")
Time of Flight	83 seconds	81.5 seconds
Flight distance	2799 m (9,190 ft.)	2789 m (9,155)
Average R_N	3.04×10^6	2.82×10^6
Average M	.10	.10
Average C_D	.714	.663

Table II Probe Model Frequencies

Probe Motion	Frequencies (cycles per second) Small Probe	Large Probe
Spin	0	.08
α	2.9 .53 .14	1.1 .14 .08
β	2.9 .47 .05	1.1 .14 .08
$\vec{\alpha} + \vec{\beta}$ (magnitude)	3.1 .31 .05	1.1 .14 .08
$\vec{\alpha} + \vec{\beta}$ (rotation)	Random	1.1